Relationship between long-range transported atmospheric black carbon and carbon monoxide at a high-altitude background station in East Asia

Shantanu Kumar Pani [a], Chang-Feng Ou-Yang [a], Sheng-Hsiang Wang [a], John A. Ogren [b], Patrick J. Sheridan [b], Guey-Rong Sheu [a], Neng-Huei Lin [a*]

[a] Cloud and Aerosol Laboratory, Department of Atmospheric Sciences, National Central University, Taoyuan 32001, Taiwan

[b] Earth System Research Laboratory, National Oceanic and Atmospheric Administration, Boulder, CO 80305, USA

*Corresponding author

Neng-Huei Lin

Cloud and Aerosol Laboratory, Department of Atmospheric Sciences, National Central University, Taoyuan 32001, Taiwan

Phone: +886-3-422-7151 ext 65531

FAX: +886-3-425-4069

E-mail: nhlin@cc.ncu.edu.tw

Abstract

Lulin Atmospheric Background Station (LABS, 23.47°N, 120.87°E; 2862 m above sea level) at the summit of Mount Lulin in central Taiwan was established in spring 2006 and is the only high-altitude background station over western Pacific region in East Asia to study the impact of various air pollutants through long-range transport. Continuous in-situ measurements of equivalent black carbon (EBC) and carbon monoxide (CO) concentrations were made at LABS from June 2012 to May 2014 and their association was investigated in this study. The highest monthly concentration of EBC (median; 840 ng m^{-3}) and CO (212 ppbv) in March were primarily attributed to the westerly winds coupled with biomass-burning (BB) emissions from Southeast Asia (SEA) region. The association of EBC and CO was weak at LABS possibly due to the influence of dissimilar air masses from various sources, and scavenging or dilution of EBC during the long-range atmospheric transport to Mt. Lulin. The mean ΔEBC/ΔCO ratio (slope of least-squares regression line of ΔEBC-ΔCO scatterplot; where Δ indicates surplus amounts with respect to the background value) was found the most significant in March (5.3 ng m^{-3} $ppbv^{-1}$ or 7.3×10^{-3} grams of carbon as EBC per gram of carbon as CO). On the basis of episodic cases, the mean ΔEBC/ΔCO ratios at LABS were estimated to be 6.1, 8.0, and 2.4 ng m^{-3} $ppbv^{-1}$ for SEA BB emissions, southern China mixed pollution, and northern China mixed pollution, respectively. A total of 32% loss in EBC aerosols (6.4% of EBC removal per day) was estimated for the atmospheric transport of BB emissions from SEA region to LABS. This study provides needful information to understand the ΔEBC/ΔCO ratios at a remote site and would be used in model simulations to evaluate BC aging and scavenging over western Pacific region in East Asia.

Keywords, Mount Lulin; Equivalent black carbon; Carbon monoxide; Long-range transport; Southeast Asia biomass-burning

1. Introduction

Black carbon (BC), an important carbonaceous component in atmospheric aerosols, is primarily formed by the incomplete combustion of carbon-containing substances including fossil fuels, biomass, and biofuels (Bond and Bergstrom, 2006; Petzold et al., 2013). BC directly absorbs the incoming solar radiation and acts as a direct radiative forcing agent (IPCC, 2013; Ramanathan and Carmichael, 2008); it also influences the lifetimes of cloud droplets and cloud microphysical properties as an indirect radiative forcing agent (Haywood and Boucher, 2000; Conant et al., 2002; Forster et al., 2007). Overall, BC aerosols can significantly influence the climate on local, regional, and global scales (Jacobson, 2001; Ramanathan and Carmichael, 2008). BC contributes significantly to the atmospheric warming (e.g., Verma et al., 2013; Pani et al., 2016a, 2016b, 2018, 2019) and is also considered as a major contributor to the global warming after carbon dioxide (CO_2) and methane (CH_4) on global scale (Ramanathan and Carmichael, 2008; Bond et al., 2013; IPCC, 2013). However, because of its non-uniform spatial and temporal distribution, BC can cause significantly higher regional forcing than CO_2 and CH_4 (Chung et al., 2005, 2010; Wang et al., 2014). BC radiative forcing with a mean value of +0.9 W m^{-2} (ranged between +0.4 and +1.2 W m^{-2}) at the top-of-atmosphere was estimated to be as much as 55% of the CO_2 forcing (Ramanathan and Carmichael, 2008). Being chemically inert and mostly concentrated in fine mode (Bond et al., 2013), BC atmospheric lifetime varies from 4 to 12 days (Cape et al., 2012) depending on the source region and meteorological conditions, and hence is subject to long-range transport (Liu et al., 2011; Wang et al., 2015).

Carbon monoxide (CO), like BC, is produced primarily from the incomplete combustion of fossil fuels and biomass (Verma et al., 2011). It is a primary trace gas but not a radiatively important gas and indirectly affects the climate through its interaction with hydroxyl radical (OH) in the

troposphere (Logan et al., 1981; Thompson, 1992; Ou-Yang et al., 2014; Okamoto and Tanimoto, 2016). OH radicals are the primary CO sink in the atmosphere. The changes in the concentration of OH radicals due to changes in CO can modify the concentrations of greenhouse gases (GHGs) like CH_4 (Thompson and Cicerone, 1986) and chlorofluorocarbons (CFCs) along with others such as hydro-chlorofluorocarbons (HCFCs) and hydrofluorocarbons (HFCs) (Okamoto and Tanimoto, 2016). The indirect radiative forcing due to CO is estimated to be 0.23 W m^{-2} (0.18–0.29 W m^{-2}) through the production of ozone (O_3), CH_4, and CO_2 (IPCC, 2013) in the atmosphere. The global mean lifetime of CO is approximately 2 months (e.g., Prather, 1996; Jennings et al., 1996) in the troposphere; however the seasonal and spatial CO lifetime variations have been reported by Duncan et al. (2007). Due to the relatively longer lifetime in the atmosphere (few weeks to 2 months), CO is a good tracer of anthropogenic pollution including burning of fossil-fuel, biomass, and biofuel and also the oxidation of hydrocarbons (Girach et al., 2014). The ocean and plants (from oxidation of biogenic hydrocarbon) are the weak natural sources of CO in the atmosphere (Finlayson-Pitts and Pitts, 2000).

Long-term measurements of BC and CO either in densely polluted or remote areas are important for better estimating the regional characteristics (Wang et al., 2006), and constraining the highly uncertain emission rate of BC (Kondo et al., 2006; Han et al., 2009; Pan et al., 2011), and also assessing the transport of BC and CO along with their effects on wide downstream regions (Verma et al., 2011). The strong positive correlation between BC and CO has been reported in several studies over distinctly different environments such as coastal, free troposphere, urban centers, and oceanic regions (Jennings et al., 1996; Chen et al., 2001; Derwent et al., 2001; Kondo et al., 2006; Andreae et al., 2008; Spackman et al., 2008; Pan et al., 2011; Verma et al., 2011; Girach et al., 2014; Kanaya et al., 2016; Guo et al., 2017). The BC/CO ratio is recognized as a good indicator to estimate the BC

93 emission following a top-to-bottom approach (Dickerson et al., 2002) and to distinguish different
94 source characteristics in case studies (Kondo et al., 2006; Spackman et al., 2008; Han et al., 2009;
95 Subramanian et al., 2010; Pan et al., 2011; Kanaya et al., 2016; Guo et al., 2017). The BC/CO ratio
96 changes significantly for different emission sources, making it a useful index to validate emission
97 inventories (Han et al., 2009; Girach et al., 2014) at near-source region. Moreover, the measurements
98 of this ratio at remote background sites (far away from sources) such as islands and high mountains
99 would be used in evaluating model treatment of BC aging and scavenging.

100 East Asia is a region where large amounts of BC are emitted. Several studies have
101 investigated the BC-CO relationship over China (e.g., Zhou et al., 2009; Verma et al., 2010; Pan et
102 al., 2011; Guo et al., 2017), Japan (e.g., Kondo et al., 2006; Kanaya et al., 2016), South Korea (e.g.,
103 Sahu et al., 2009), western north Pacific rim (e.g., Verma et al., 2011), and Taiwan (e.g., Chou et al.,
104 2010). However, situated far away from the anthropogenic or biomass-burning (BB) source-
105 emissions, high-altitude mountain stations are considered to be ideal sites for monitoring the
106 temporal/seasonal variations of aerosols and trace gases in the atmosphere at background levels
107 (Okamoto and Tanimoto, 2016). These sites also allow for continuous observations at high-altitude
108 often in the free tropospheric zone (e.g., Freney et al., 2016; McClure et al., 2016; Shen et al., 2016;
109 Ou-Yang et al., 2017). This present study focuses on continuous measurements of BC and CO at a
110 high-altitude regional background site in East Asia, i.e., Mount Lulin in central Taiwan. Even though
111 the seasonal variation of elemental carbon (EC; Chuang et al., 2014) and CO (Ou-Yang et al., 2014)
112 have been reported at Mt. Lulin by using long-term and multi-year datasets, their associations are not
113 yet thoroughly investigated and well understood. In this current study, we mainly discuss the
114 monthly/seasonal variations of BC and CO mass concentrations and their ratios at the summit of Mt.
115 Lulin in East Asia.

2. Instrumentation and measurements

2.1. Brief description about the observational site

The focus observational site (Fig. 1) in this present study is the Lulin Atmospheric Background Station (LABS; 23.47°N, 120.87°E; 2862 m above sea level, a.s.l.) at the summit of Mt. Lulin, Taiwan (http://lulin.tw/en/). LABS is a two-story building situated at the peak of Mt. Lulin in Yushan National Park (http://www.ysnp.gov.tw/en/) in central Taiwan. LABS is the first high-altitude background station in East Asia and complements the Global Atmospheric Watch (GAW) network. This site is 2 km away from the nearest minor traffic road and there are no significant known emissions of BC or CO in the proximity of the site. Owing to the geographical features, the LABS frequently lies within the free troposphere and is an ideal site to conduct measurements to study the impact of air pollutants resulting from both regional sources and those arriving at the site via long-range transport (e.g., Sheu et al., 2010; Lee et al., 2011; Ou-Yang et al., 2012; 2014; Chuang et al., 2014; Pani et al., 2017; Park et al., 2018, 2019).

2.2. Measurements

An aerosol observation system (AOS) was built by the National Oceanic and Atmospheric Administration (NOAA, USA) at LABS. Continuous measurements of meteorological parameters, solar radiation, trace gases, and aerosol properties have been operational since spring of 2006 (Sheu et al., 2010). Light absorption and scattering measurements were added to the suite of instruments in the autumn of 2008 (Andrews et al., 2011). The detailed description about the NOAA AOS can be found elsewhere (Sheridan et al. 2001; Delene and Ogren, 2002; Hsiao et al., 2017; Andrews et al., 2019).

The equivalent BC (eBC; Petzold et al., 2013) determinations were made from June 2012 to May 2014 at LABS using an aethalometer (AE, Model AE-31; Magee Scientific, Berkeley, CA USA)

which measures changing light attenuation through an aerosol-laden filter. Sample air was obtained from the top of the sampling stack (~10 m above ground level) with a PM_{10} cyclone (cut-off diameter of 10 µm) size-selective inlet with a protective rain cap. A heater was attached to control the relative humidity to less than 40% (RH < 40%) to minimize any hygroscopic effects. AE-31 performs continuous determinations of light absorption coefficient (σ_{ap}) at seven different wavelengths (370, 470, 520, 590, 660, 880, and 950 nm). The principle of AE-31 determines σ_{ap} by quantifying the attenuation of light transmitted through the sample spot on a quartz fiber filter (Hansen et al., 1984). The eBC mass concentrations (in ng m^{-3}) were estimated from the σ_{ap} (in Mm^{-1}) using a wavelength-dependent specific mass absorption cross-section (MAC) value of 16.6 m^2 g^{-1} at 880 nm and as follows (Bodhaine, 1995; Weingartner et al., 2003).

$$eBC = \frac{\sigma_{ap} \times C \times R \times 1000}{16.6} \qquad (1)$$

The eBC measurement at 880 nm is considered as standard because BC is the principal absorber of light at this wavelength and other aerosols have negligible absorption at this wavelength (Hansen et al., 1984; Bodhaine, 1995; Weingartner et al., 2003; Verma et al., 2013, Pani, 2013; Pani and Verma, 2014). This MAC value of 16.6 m^2 g^{-1} at 880 nm is also recommended by the manufacturer for AE-31 measurements to account for absorption by BC and additional light scattering by both particles and filter fibers (Xu et al., 2017; Sharma et al., 2017). However, the use of factory calibrated MAC value of 16.6 m^2 g^{-1} may lead to some uncertainty, because MAC varies anywhere between 5 and 25 m^2 g^{-1} for various locations (Liousse et al., 1993, Petzold et al., 1997, Weingartner et al., 2003; Bond and Bergstrom, 2006). Uncertainties involved in the eBC measurements using an AE are reported in literatures (Weingartner et al., 2003; Arnott et al., 2005; Sheridan et al., 2005; Corrigan et al., 2006; Schmid et al., 2006; Virkkula et al., 2007; Collaud Coen et al., 2010; Backman et al., 2017). Filter-

161 based absorption method in AE has two known impediments that interfere with measurement
162 accuracy (Arnott et al., 2005; Corrigan et al., 2006). These interferences must be considered in order
163 to obtain reliable σ_{ap} and BC mass (Sheridan et al., 2005; Corrigan et al., 2006). Firstly, the
164 amplification factor arising from multiple scattering of light in the quartz filter fiber matrix and is
165 commonly termed as "C-factor" (Weingartner et al., 2003). Secondly, the change in the optical path
166 length due to successive filter loading (shadowing effect) and is commonly termed as "R-factor"
167 (Weingartner et al., 2003; Arnott et al., 2005). In Equation (1), C is the enhancement parameter
168 which accounts for the multiple scattering and strongly depends on the filter material (C = 2.81;
169 Weingartner et al., 2003) and R is the correction for shadowing effect (R = 1; Weingartner et al.,
170 2003). Andrews et al. (2011) also used the same C = 2.81 value for the correction of σ_{ap}
171 measurements at a high-alpine research station in Jungfraujoch, Switzerland. The shadowing effect
172 has been found to be more prominent for pure soot (BC) particles but almost negligible for aged
173 aerosols (Weingartner et al., 2003). The aged aerosol concept applies well to our sampling site
174 LABS. Moreover, this study utilizes the hourly averaged and quality-checked σ_{ap} measurements to
175 determine eBC and the temporal averaging can significantly lessen the measurement uncertainty and
176 noise (Jefferson, 2011). Filter-based absorption photometers are normally considered to be accurate
177 within 20–30 % of the true σ_{ap} value (Bond et al., 2013). The accuracy is a combination of
178 instrument noise, variability, and calibration uncertainty (e.g. Sherman et al., 2015; Backman et al.,
179 2017).

180 The AE-31 was set to function at a standard mass flow rate (V_0) of 4 liter per minute (LPM)
181 under standard temperature and pressure (STP, T_0 = 273.15 K and P_0 = 1013.25 hPa) condition.
182 However, the ambient pressure being lower than the standard condition, AE-31 samples aerosols
183 with higher pumping speed in order to maintain the set mass flow rate, and hence more volume of air

184 gets aspirated. Hence, the actual volume (V) of ambient air aspirated at an ambient temperature (T)
185 and pressure (P) was,

186 $$V = V_0 \times \frac{P_0}{P} \times \frac{T}{T_0} \quad (2)$$

187 Since the eBC concentrations were calculated based on V_0, the eBC concentration at ambient
188 conditions (EBC) was estimated as follows (e.g., Moorthy et al., 2004; Babu et al., 2011)

189 $$EBC = eBC \times \left[\frac{P_0 \times T}{P \times T_0}\right]^{-1} \quad (3)$$

190 Following the equation (3), each measurements of eBC were converted to the EBC concentrations.
191 The accuracy of EBC concentrations measured by AE-31 has been estimated to be ~20% as
192 compared to thermal-optical reflectance (TOR) based EC concentrations measured at Mt. Lulin (e.g.,
193 Chuang et al., 2014, 2016b).

194 Simultaneous and continuous measurements of CO concentrations were obtained from an in-
195 situ non-dispersive infrared spectrometer (NDIR; APMA-360, Horiba, Japan) with a flow rate of 1.2
196 LPM (at ambient temperature and pressure condition) at a frequency of 6 second and further
197 calculated into hourly averages. The detection limit of the NDIR is ~20 ppb (1σ; Zellweger et al.,
198 2009) and the overall statistical uncertainty is calculated to be ±14.4 ppb based on the mean standard
199 deviation of the 6 s data within each hour in this current study. The calibration details of the NDIR
200 instrument have been discussed in Ou-Yang et al. (2014).

201 In order to make source-receptor analysis, EBC and CO measurements made (following the
202 same instrumentation and methodologies as discussed above) at an upwind near-source BB location
203 in northern SEA i.e., Doi Ang Kang Meteorology Station (DAK), Chiang Mai Province, Thailand
204 (19.93°N, 99.05°E, 1536 m a.s.l.) during March 2013 as part of the Seven South East Asian
205 Studies/Biomass-burning Aerosols & Stratocumulus Environment: Lifecycles & Interactions

206 Experiment (7-SEAS/BASELInE; Lin et al., 2014; Tsay et al., 2016) campaign were also included in
207 this current study.

208 **3. Results and discussion**

209 *3.1. Local meteorology and air mass back trajectories*

210 Monthly meteorological parameters (mean ± 1σ) obtained from hourly measurements of
211 temperature (T), relative humidity (RH), wind speed (WS), and rainfall at LABS are presented in
212 Figs. 2a-d. Monthly mean T (Fig. 2a) varies in between 6 °C (January) and ~14 °C (July) with an
213 annual mean (± 1σ) value of 10 ± 4 °C. RH was generally high (> 60%) throughout the observation
214 period with an annual mean (± 1σ) value of 79 ± 25%, varying from January (62%) to May (94%) as
215 shown in Fig. 2b. The annual WS (mean ± 1σ) was about 3.9 ± 2.5 m s^{-1} with the lowest (Fig. 2c) in
216 September (2.1 ± 1.3 m s^{-1}) and the highest in December (5.5 ± 2.8 m s^{-1}). Hourly rainfall data was
217 obtained from an automatic rain gauge installed in the LABS premises and the monthly rainfall (Fig.
218 2d) was ranged between 36 mm (January) and 1455 mm (August). Monthly mean surface pressure
219 (P) was varied between 722–726 hPa at LABS. According to the classification given by previous
220 studies depending on local meteorological conditions (e.g., Wai et al., 2008; Ou-Yang et al., 2012,
221 2014), LABS experiences four distinct seasons, namely summer (June, July, and August), fall or
222 autumn (September, October, and November), winter (December, January, and February), and spring
223 (March, April, and May). The seasonal variability of meteorological parameters along with their
224 statistical analysis is listed in Table 1.

225 LABS generally receives air masses that have originated/passed over China, India, cleaner
226 maritime regions, and also from SEA BB emissions (e.g., Lee et al., 2011; Lin et al., 2013; Ou-Yang
227 et al., 2014). In order to better understand the influence of heterogeneity in air masses during the
228 observation period, 5-day air mass backward trajectories (BTs) ending at ground level (altitude =

2862 m a.s.l) of LABS at 00/06/12/18 UTC daily (i.e., 4 BTs per day) have been computed by using the Hybrid Single Particle Lagrangian Integrated Trajectory (HYSPLIT; Draxler and Rolph, 2013) model. Fig. 3 shows the monthly relative frequency (%) distributions (e.g., Pani and Verma, 2014; Verma et al., 2014, 2016) for different possible pathways from June 2012 to May 2014. The intensity of BB emissions in East Asia, South Asia, and SEA (as shown in Fig. 3) were illustrated by fire counts obtained from the Moderate Resolution Imaging Spectroradiometer (MODIS) Collection 5 near real-time Hotspot/Active Fire Detections (MCD14DL) using the Terra/Aqua satellites (https://earthdata.nasa.gov/data/near-real-time-data/firms/). During the spring, air masses carry mainly continental BB emissions from SEA to the sampling site in the Pacific by a long-range atmospheric transport (*cf.* Lee et al., 2011). The LABS gets the air masses from oceanic area and free troposphere higher than 700 hPa over the Asian continent (*cf.* Lee et al., 2011) during the summer. In autumn, the northwesterly air mass pattern carries continental anthropogenic-pollutants, dusts, and BB emissions from East Asia to the sampling site by a long-range atmospheric transport. In winter, the air mass pattern shifts majorly from northwesterly to southwesterly with stronger winds towards February.

3.2. EBC mass concentrations

The annual mean (± 1σ) EBC concentration was found to be 275 ± 406 ng m^{-3}, with the median value of 117 ng m^{-3}, at LABS during the whole observation period. The monthly EBC mass concentration (mean ± 1σ; Fig. 4a) started increasing from June (60 ± 64 ng m^{-3}) until October (220 ± 169 ng m^{-3}), then suddenly decreased in November (89 ± 107 ng m^{-3}), followed by an increasing trend to reach the annual maximum in March (883 ± 621 ng m^{-3}) and then started decreasing again to June. The bimodal distribution of EBC concentrations with the major mode in March and relatively less pronounced minor mode in October were related to the insignificant wet removal of EBC due to

low RH (Fig. 2b) and rainfall (Fig. 2d) during these two months. EBC mean concentration varied approximately fifteen-fold from the lowest in June to the highest in March during the observation period. The highest mass concentration of EBC in March (median = 840 ng m^{-3}) was primarily attributed to the influence of westerly winds coupled with BB emissions from SEA. It can be explained with the analysis of air mass BTs and MODIS fire count data during March (Fig. 3), which clearly showed that air masses were frequently coming from the peninsular SEA (Vietnam, Cambodia, Thailand, Laos, and Myanmar, etc.) where intense BB was occurred particularly in March. The secondary peak during October was linked with the influence of Asian continental outflows in conjunction with BB emissions from north/northeastern/southern China (Fig. 3). Pani et al. (2017) recently reported the influence of Asian continental outflows to the surface mass concentration of EC at Mt. Lulin during an intensive observational period (IOP) in winter of 2015. Ambient aerosols were greatly influenced by the agriculture crop residue burning in northern China during late September to early November (You et al., 2015). Moreover, the prevalence of dry weather since late autumn in most parts of northern China (Zhai et al., 2005) increases the forest and grassland fire activities (You et al., 2015). Pan et al. (2011) also reported higher concentration of EBC in October than the summer months at Mt. Huang, China, consistent with the large-scale burning of crop residues over the region.

The seasonal statistics of EBC concentrations measured at LABS are also summarized in Table 1. The highest EBC concentration (mean ± 1σ; median) was found in spring (563 ± 585 ng m^{-3}; 348 ng m^{-3}), followed by winter (252 ± 295 ng m^{-3}; 140 ng m^{-3}), autumn (152 ± 148 ng m^{-3}; 104 ng m^{-3}), and summer (68 ± 71 ng m^{-3}; 39 ng m^{-3}). BB aerosols produced in the SEA region consistently influenced the LABS atmosphere with the domination of westerlies (e.g., Hsiao et al., 2017). BB emissions are the notable component of global combustion-sourced BC and contributing

up to 63% (Bond et al., 2004; Lack et al., 2012). Significant contribution of SEA BB emissions to springtime concentration of air pollutants including $PM_{2.5}$ (cut sizes ≤ 2.5 μm), EC, O_3, and gaseous elemental mercury at LABS were also reported in literatures (e.g., Wai et al., 2008; Sheu et al., 2010; Lee et al., 2011; Ou-Yang et al., 2012; Lin et al., 2013; Chuang et al., 2014, 2016a, 2016b). Moreover, springtime regional transport of SEA BB emissions has been also well investigated over downwind sites in East Asia e.g., southeastern China, South China Sea, and central/southern Taiwan (Lin et al., 2013; Pani et al., 2016a). Like LABS, the highest EBC during spring season was also reported at various high-altitude locations i.e., NCOP, Nepal (altitude, 5079 m; reference, Marinoni et al., 2010), Hanle (4520 m; Babu et al., 2011), Mukteshwar (2180 m; Hyvärinen et al., 2009), Manora Peak, Nainital (1958 m; Dumka et al., 2010), Dehradun (700 m; Babu et al., 2011), and Mauna Loa, Hawaii, USA (3400 m; Bodhaine, 1995), irrespective of mass concentrations, measurement methods, applied corrections, and source origins. The lowest EBC concentration during summer season was primarily caused by the frequent intrusions of clean marine air mass from the Pacific and South China Sea (Fig. 3) and these air masses were also reported as responsible for the seasonal minimum of other air pollutants including CO and O_3 at LABS (Sheu et al., 2010; Lee et al., 2011; Ou-Yang et al., 2012, 2014). In addition to the above fact, wet removal was also another key factor of BC declination during the summer months due to higher rainfall (Fig. 2d).

Table 2 summarizes the mean EBC mass concentrations measured at LABS with other high-altitude locations in the world. The annual mean EBC (275 ng m^{-3}) at LABS was found comparable with the values reported at Tengchong county (Engling et al., 2011), Mt. Waliguan (Ma et al., 2003), and NCO-P (Marinoni et al., 2010) but relatively higher (~3 to 6) times than those at Hanle (Babu et al., 2011), Nam Co (Zhang et al., 2017), and Qilian Shan (Zhao et al., 2012). The annual mean EBC at Godavari (Engstrom and Leck, 2017); Ooty (Udayasoorian et al., 2014), Manora Peak (Dumka et

298 al., 2010), Mt. Huang (Pan et al., 2011), and Darjeeling (Sarkar et al., 2015) was found to be 2, 2, 4,
299 4, and 13 times higher than that of LABS, respectively. The mean EBC during March (883 ng m^{-3}) at
300 LABS was found comparable with the values reported at Linzhi (Cao et al., 2010) and Sinhagad
301 (Raju et al., 2011) whereas 6 times lower than that reported at DAK (Hsiao et al., 2016).

302 *3.3. CO concentrations*

303 The annual mean (± 1σ) and median value of CO concentration was found to be about 140 ±
304 52 ppbv and 129 ppbv, respectively at LABS during the whole observation period. Monthly CO
305 concentrations (mean ± 1σ; Fig. 4b) varied similarly as EBC mass concentrations. Similar to EBC
306 seasonal variation, CO concentration (mean ± 1σ; median) was also observed as the highest in spring
307 (167 ± 74 ppbv; 150 ppbv), followed by the winter (142 ± 39 ppbv; 137 ppbv), autumn (135 ± 36
308 ppbv; 130 ppbv), and summer (104 ± 27 ppbv; 95 ppbv) at LABS (Table 1). Ou-Yang et al. (2014)
309 also reported the similar pattern of seasonal CO variations from April 2006 to April 2011 at LABS.
310 The CO seasonal pattern at LABS was also found similar with those reported at other sites in western
311 Pacific (Narita et al., 1999; Pochanart et al., 2004; Tsutsumi et al., 2006; Kim et al., 2008;
312 Suthawaree et al., 2008; Yashiro et al., 2009; Sikder et al., 2011) regardless of the slight differences
313 in concentration. Relatively higher CO during the autumn and winter months at LABS was observed
314 due to the influence of Asian continental outflows. The highest level of CO in spring was primarily
315 attributed to the westerly air masses in conjunction with BB emissions from SEA. The influence of
316 intense BB emissions from SEA was also reported at Mt. Bachelor observatory (MBO; 2763 m a.s.l.)
317 in central Oregon, USA (Reidmiller et al., 2009). However, higher springtime CO concentrations
318 (203–227 ppbv) were often reported mainly due to the influence of Asian continental outflows at the
319 coastal sites in western Pacific such as Hoppo (Narita et al., 1999), Cape Hedo (Suthawaree et al.,
320 2008), and Oki (Sikder et al., 2011). High levels of CO produced in SEA passing over the Pacific in

springtime were also detected by the MOPITT (Measurement of Pollution in the Troposphere) satellite (Deeter et al., 2009). On the basis of STEM (Sulfur Transport and dEposition Model) tracer simulations, the spreading of BB-produced CO from SEA over the west coast of Pacific at an elevation of ~2.8 km was reported during the TRACE-P (Transport and Chemical Evolution over the Pacific) experiment (Tang et al., 2003).

3.4. Possible impact of local emissions on EBC and CO concentrations

Even though the monthly and seasonal concentrations of EBC and CO at LABS are mainly governed by the long-range atmospheric transport from continental outflows as discussed in earlier sections, the influence of local/regional emissions cannot be completely ignored. Primary air pollutants accumulated in the planetary boundary layer (PBL) of nearby suburban/urban areas can be transported to LABS by mountain–valley (M–V) circulation primarily depending on the vertical profiles of meteorological parameters as well as air-pollutants and the height of atmospheric mixing layer. Some earlier studies discussed the influence of M–V circulations and upslope winds on the diurnal variations (daytime minimum around noon and nighttime maximum) of CO, O_3, $PM_{10,}$ and gaseous elementary mercury at LABS (Sheu et al., 2010; Ou-Yang et al., 2012, 2014). Oltmans and Komhyr (1986) also suggested that the up-down slope circulations were responsible for the similar diurnal pattern in O_3 observed at Mauna Loa in Hawaii on the basis of vertical profiles of O_3 and meteorological data. Ou-Yang et al. (2014) has elaborately discussed the influence of M–V circulation on CO diurnal variations in different seasons at LABS and also found the M–V winds as the major cause of daily CO maximum in afternoon along with water vapor levels. Therefore, it is possible that the local/regional emissions accumulated in PBL of nearby valley may occasionally influence the diurnal/daily variations of EBC concentrations at the altitude of LABS (~3 km) by upslope winds during the favorable meteorological conditions.

3.5. EBC and CO relationship

The relationship between EBC and CO is primarily regulated by the balance between sources and sinks (Spackman et al., 2008). The sources are mainly governed by the fuel type and combustion efficiency (Miguel et al., 1998; Bond et al., 2004) whereas the sinks are governed by meteorological conditions and atmospheric aging. It is important to mention that CO is insoluble in water and is not removed by precipitation. In contrast, during the atmospheric transport process BC particles undergo a transformation from hydrophobic to hydrophilic by forming an internal mixture with sulfate and organic components which enhances BC removal by wet deposition and sedimentation (Spackman et al., 2008). Low values (0–0.56) of Pearson correlation coefficient (r) of EBC-CO scatterplots (supplemental Fig. S1) were due to the influence of dissimilar air masses from various source origins to Lulin's remote atmosphere through long-range atmospheric transport process. This mix of sources may contribute to the non-linearity in the EBC-CO correlation (e.g., Spackman et al., 2008). A strong correlation between EBC and CO can be expected over the near-source region of emissions (e.g. anthropogenic or BB), but the atmospheric long-range transport makes the association weaker at remote locations (Sahu et al., 2009).

Generally, the EBC and CO relationship is represented as ΔEBC/ΔCO ratio (e.g., Kondo et al., 2006; Spackman et al., 2008; Pan et al., 2011; Verma et al., 2011; Girach et al., 2014; Kanaya et al., 2016) and this ratio is used to identify the factors that control variations in BC mass concentration (Kanaya et al., 2016). In this current study, ΔEBC and ΔCO represent the differences between observed and background values of EBC and CO concentrations, respectively. EBC_0, the background concentration of EBC was assumed to be zero (e.g., Pan et al., 2011; Kanaya et al., 2016; Kondo et al., 2016) because the estimated atmospheric lifetime of BC is several days (e.g., Cooke et al., 2002; Park et al., 2005; Bond et al., 2013; Kondo et al., 2016); hence ΔEBC was the

same as the original EBC concentration. However, CO_0 (the background concentration of CO) was determined as the median of the values below the 3σ range, namely the 1.25th percentile of the CO concentrations for each month (e.g., Kondo et al., 2006; Pan et al., 2011; Girach et al., 2014). The monthly CO_0 values are also presented in Fig. 4b along with the CO concentrations. Some studies have used the slope of the least squares fitting of EBC-CO scatterplots as ΔEBC/ΔCO ratio (e.g., Kondo et al., 2006; Han et al., 2009; Guo et al., 2017). However, we used the slope of the least squares fitting of ΔEBC-ΔCO scatterplot as ΔEBC/ΔCO ratio (e.g., Kondo et al., 2006, 2011) in this current study for more accurate estimation at our remote background site.

Fig. 5 shows the monthly scatterplot and linear regression results of the ΔEBC-ΔCO correlation at LABS. The regression model was found statistically significant ($p < 0.05$) during all the moths except October ($p = 0.337$). However, the correlation between ΔEBC and ΔCO (Fig. 5) was found very-weak (i.e., < 0.2) during July, October, November, and May; weak (i.e., < 0.3) during June and September; and moderate (i.e., $r > 0.3$) during remaining months. Although a secondary peak in both EBC and CO concentrations was seen on October along with the lower RH and rainfall, but the weakest association ($r = 0.003$) between ΔEBC and ΔCO (as well as insignificant statistical regression) was probably due to the influence of dissimilar air masses from various distinct source origins (as seen from the Fig. 3). The discussion of ΔEBC/ΔCO ratios is not meaningful for the months when ΔEBC-ΔCO correlations were very-weak and weak. Therefore, the statistical results of ΔEBC-ΔCO scatterplots with moderate correlation are listed in Table 3 and discussed here. The ΔEBC/ΔCO ratio (mean ± standard error at 95% confidence interval) was found to be significant particularly in the springtime with the highest in March (5.3 ± 0.3 ng m^{-3} $ppbv^{-1}$) with closely similar to February (4.1 ± 0.3 ng m^{-3} $ppbv^{-1}$) and followed by April (3.1 ± 0.2 ng m^{-3} $ppbv^{-1}$). Relatively higher ΔEBC/ΔCO ratios in spring months were attributed to the significant

influence of BB emissions from the South Asia and SEA to the LABS atmosphere through long-range transport with westerlies winds (as seen from the Fig. 3). Substantial BB occurs annually from February to April over SEA region due to land-clearing practices before the local growing season (Khamkaew et al., 2016; Hsiao et al., 2016; Tsay et al., 2016; Pani et al., 2016b, 2018). Low value of ΔEBC/ΔCO ratio in August (1.7 ± 0.1 ng m^{-3} $ppbv^{-1}$) at LABS was due to more complete EBC removal as result of the highest occurred rainfall (1455 mm; Fig. 2d) and possible contributions of CO from volatile organic compounds (VOC) oxidation (e.g., Spackman et al., 2008). Relatively lower value of ΔEBC/ΔCO ratio during December (1.3 ± 0.1 ng m^{-3} $ppbv^{-1}$) was due to the combine effect of scavenging of EBC by RH (80 ± 26%) and rainfall (318 mm) and influence of different air masses (Fig. 3). Although the rainfall (36 mm) and RH (62 ± 34%) were recorded the lowest during January, still the ΔEBC/ΔCO ratio was observed low possibly due to poor association between EBC and CO as a result of mixing of air masses originating from different source origins (Fig. 3). However, the ΔEBC/ΔCO ratio in January (2.1 ± 0.2 ng m^{-3} $ppbv^{-1}$) was relatively higher as compared to August and December due to higher EBC mass in January (Fig. 4a) than August and December at LABS. The ΔEBC/ΔCO ratios estimated at Mt. Lulin represent well mixed air masses from different regions owing to long-range atmospheric transport and here in this study referred to a typical value on a regional scale in contrast with the ratios of any specific emission types.

3.6. Episodic cases of ΔEBC/ΔCO enhancement

Three episodic cases, when the ΔEBC-ΔCO correlation was more significant as compared to the respective monthly scatterplot, were selected to determine the ΔEBC/ΔCO ratios for particularly BB emission and/or urban mixed pollution. Figs. 6a-c shows the statistical results of ΔEBC-ΔCO scatterplots for the episodic cases and relatively strong correlations ($r > 0.65$) for each episode were observed. During 28–31 March, 2013 (Case#1), BB air masses were particularly coming from the

413 northern SEA to the LABS as depicted by 5-day BT information (Fig. 7a). The vertical distribution
414 of aerosol subtype, obtained from the Cloud-Aerosol Lidar and Infrared Pathfinder Satellite
415 Observations (CALIPSO; https://www-calipso.larc.nasa.gov) web application, displayed the
416 presence of thick smoke plumes at 1–5 km altitude distributed over 10°N – 25°N in East Asia on 28
417 March 2013 (Fig. 7d). Interestingly, the aerosol optical depth at 500 nm was also recorded as the
418 highest (0.73) by the Cimel sun–sky radiometer of Aerosol Robotic Network (AERONET;
419 http://aeronet.gsfc.nasa.gov/) at Mt. Lulin (supplemental Fig. S2) on that particular day and was
420 found to be approximately 5 times higher than the monthly mean (0.14) of March 2013. EBC and
421 CO concentrations at LABS for Case#1 had means of 724 ng m^{-3} and 207 ppbv, respectively and the
422 CO_0 value was 96 ppbv. The ΔEBC/ΔCO ratio (mean ± standard error at 95% confidence interval)
423 for Case#1 was found to be 6.1 ± 0.7 ng m^{-3} $ppbv^{-1}$ i.e., ~1.2 times higher than that of overall
424 monthly mean of March (5.3 ± 0.3 ng m^{-3} $ppbv^{-1}$).

425 Taiwan generally receives the Asian continental outflow during October–November (Pani et
426 al., 2017; Chuang et al., 2017). Two cases, when mixed urban pollution from Asian continental
427 outflow played a dominant role on high EBC mass concentrations at LABS, were also selected.
428 Case#2 (30 October 2013) was mainly attributed to the mixed pollution of urban and BB emissions
429 from southern China as seen from the 5-day BT information (Fig. 7b) and vertical distribution of
430 aerosol subtype (Fig. 7e). Agricultural residue burning attributed to the burning of rice straw after
431 rice harvest is reported over southern and east China particularly during October (e.g. Pan et al.,
432 2011; Chen et al., 2017). During Case#2, CO_0 value was 97 ppbv, and the mean CO (131 ppbv) was
433 found ~1.2 times lower than that of monthly mean of October (153 ppbv) while the mean EBC (250
434 ng m^{-3}) was found ~1.1 times higher than that of monthly mean of October (220 ng m^{-3}), resulting in
435 the overall enhanced value of ΔEBC/ΔCO ratio about to be 8.0 ± 2.1 ng m^{-3} $ppbv^{-1}$. On 28

November 2013 (Case#3), another episode of continental Asian outflow was observed and mainly attributed to mixed pollution of urban and BB emissions from northern China as seen from the 5-day BT information (Fig. 7c) and vertical distribution of aerosol subtype (Fig. 7f). During Case#3, the EBC and CO concentration (mean ± 1σ) was 109 ± 35 ng m^{-3} and 131 ± 11 ppbv, respectively, CO_0 was 111 ppbv, and ΔEBC/ΔCO ratio was 2.4 ± 0.6 ng m^{-3} $ppbv^{-1}$ i.e., ~6–7 times higher than that of overall monthly mean of November (0.4 ± 0.1 ng m^{-3} $ppbv^{-1}$). The difference in ΔEBC/ΔCO ratios for Case#1, Case#2, and Case#3 was possibly due to the different emissions strengths over the upwind locations i.e., SEA, southern and northern China, respectively. Although, the mean CO values were same for Case#2 and Case#3, the mean EBC of Case#3 was ~2.3 times lower than that of Case#2. It was possibly due to some EBC removal by significant RH (95%) and rainfall (total rainfall = 4.3 mm; supplemental Fig. S3) on that particular day of Case#3. Additionally, the presence of thick continental polluted dust at 1–3 km atmospheric altitude over the region (as seen from CALIPSO satellite results; Fig. 7f) was another important reason of EBC dilution during Case#3 at LABS. However, there was no rainfall recorded for Case#2 and the mean RH was 60%. As a result, the ΔEBC/ΔCO ratio at LABS for the mixed pollution from southern China (Case#2) was found to be ~3 times higher than that of northern China (Case#3).

However, such large standard error associated with the mean value of ΔEBC/ΔCO ratios for the episodic cases (Figs. 6a-c), may bias the discussions of observed enhancement. Therefore for re-examination, we again derived the ΔEBC/ΔCO ratio by considering the median value of the ratios of each data point i.e., using the equation $\frac{\Delta EBC}{\Delta CO} = (EBC - EBC_0)/\,(CO - CO_0)$ following Kondo et al., (2006, 2016). The estimated median value of ΔEBC/ΔCO ratios for Case#1 (6.2 ng m^{-3} $ppbv^{-1}$) and Case#2 (8.1 ng m^{-3} $ppbv^{-1}$) were found closely identical with the mean values of the slope of ΔEBC-

458 ΔCO scatterplots (Figs. 6a-b), indicating that datasets were followed normal distribution in both the
459 cases. However, the median value of ΔEBC/ΔCO ratio for Case#3 was estimated to be 5.1 ng m^{-3}
460 $ppbv^{-1}$ i.e., about ~2 times higher than the mean value of the slope (2.4 ± 0.6 ng m^{-3} $ppbv^{-1}$) of
461 ΔEBC-ΔCO scatterplot (Fig. 6c), indicating non-normal distribution of the dataset including some
462 major outliers at the both end of the distribution. It could be due to two reasons (i) low values of
463 EBC due to wet removal as well as dust contamination and (ii) the low values of ΔCO due to high
464 magnitude of CO_0 (111 ppbv), which was even higher than the mean EBC (109 ng m^{-3})
465 concentration for Case#3.

466 *3.7. Comparison of ΔEBC/ΔCO ratio with other studies*

467 Fig. 8 summarizes the ΔEBC/ΔCO ratios reported by some previous studies at different
468 locations worldwide as well as the variations between BB emissions and urban plume. It is worth to
469 note here that the summarized ΔEBC/ΔCO ratios for comparison purpose (Fig. 8) are based on
470 several measurement procedures with different errors and uncertainties. An extensive inter-
471 comparison of measurement procedures and their uncertainties are beyond the scope of this paper
472 and the reader can follow the corresponding references for the details. The ΔEBC/ΔCO ratio of 11.5
473 ng m^{-3} $ppbv^{-1}$ for local scale BB episode at Mt. Cimone in Italy (2165 msl; Cristofanelli et al., 2013)
474 was ~2 times higher than the value of BB episode at Mt. Lulin (6.1 ± 0.7 ng m^{-3} $ppbv^{-1}$). Pan et al.
475 (2011) also reported the higher values of ΔEBC/ΔCO ratio of ~10.3–11.6 ng m^{-3} $ppbv^{-1}$ for BB
476 episodes in the high-altitude environment of Mt. Huang in eastern China. Regional Emission
477 inventory in Asia also reported ΔEBC/ΔCO ratios of 11.0, 11.4, 11.0, and 11.8 ng m^{-3} $ppbv^{-1}$ for
478 open BB of agricultural residue in Anhui, Jiangsu, Shandong, and Henan provinces, respectively
479 (Yamaji et al., 2010). Recently, Guo et al. (2017) studied the ΔEBC/ΔCO ratios and found lower
480 values over Beijing and Changdao Island in northern China than those over Nanjing, Shanghai,

Wenling, and Guangzhou in South China, due to disparate fuel structures in North and South China. Higher values of ΔEBC/ΔCO ratio for South China air-mass than that of North China air-mass was reported at Mt. Huang, eastern China (Pan et al., 2011), Cape Hedo, Okinawa, northern Pacific rim (Verma et al., 2011), and Fukue Island, western Japan (Kanaya et al., 2016). However, the lower ΔEBC/ΔCO ratios obtained over megacities such as Beijing and Shanghai were due to the higher number of gasoline and diesel vehicles (Zhou et al., 2009). McMeeking et al. (2010) estimated the ΔEBC/ΔCO ratios ranging between 0.8–6.2 ng m^{-3} $ppbv^{-1}$ in the boundary layer over Europe. Jaffe et al. (2017) reported the ΔEBC/ΔCO ratios ranging from 3.29–4.98 ng m^{-3} $ppbv^{-1}$ at Mount Bachelor Observatory site in central Oregon, USA during the influence of wildfire events. The association between EBC and CO is highly region specific. In general, the variation of ΔEBC/ΔCO ratios were found between different studies are because of their emission ratios, fuel types, combustion efficiencies, secondary formation of CO from VOC oxidation (Bond et al., 2004; McMeeking et al., 2010), and meteorological conditions (Oshima et al., 2012).

3.8. Transport efficiency of EBC for SEA BB emissions at Mt. Lulin

The transport efficiency (TE) of EBC was estimated relative to CO (long-lived and relatively an inert species) in order to investigate the BC atmospheric transport to Mt. Lulin. TE is also used to characterize the extent to which the wet deposition of EBC occurs during the atmospheric transport (Kondo et al., 2016). TE was estimated in this current study as follows (Park et al., 2005; Sahu et al., 2009; Girach et al., 2014; Kondo et al., 2016)

$$\mathrm{TE}\ (\%) = \frac{(\Delta \mathrm{EBC}/\Delta \mathrm{CO})}{(\mathrm{ER}_{\mathrm{EBC/CO}})} \times 100 \qquad (4)$$

where $\mathrm{ER}_{\mathrm{EBC/CO}}$ is the emission ratio of EBC to CO in the source region.

Dilution and aging effects on EBC and CO are negligible over the source regions (e.g.,

503 Baumgardner et al., 2002; Girach et al., 2014). Therefore, we considered $ER_{EBC/CO}$ ratio at DAK (a
504 near-source BB region in northern SEA) as the representative value for SEA BB emissions. EBC
505 (23–26 March, 2013) and CO (24–31 March, 2013) concentration (mean ± 1σ) at DAK was found to
506 be about 5290 ± 1142 ng m^{-3} and 594 ± 79 ppbv, respectively. The mean $ER_{EBC/CO}$ value was
507 estimated to be 8.9 ng m^{-3} $ppbv^{-1}$ (or 15.3×10^{-3} grams of carbon as EBC per gram of carbon as CO)
508 at DAK and by using this value the TE of EBC for SEA region BB air mass (Case#1, 28–31 March,
509 2013) was estimated about to be ~68%. This result reveals that springtime EBC aerosols from SEA
510 region were transported efficiently to Mt. Lulin, though scavenging effect due to RH and rainfall was
511 observed at LABS, Mt. Lulin. It is worth to mention here that the total rainfall was 20 mm and the
512 mean RH was 95% at LABS during 28–31 March 2013 (Case#1). A total of 32% loss in EBC was
513 occurred due to the dry as well as wet deposition (through both rain and high RH) during the
514 atmospheric transport process from SEA region to LABS (i.e., 2400 km in 5 days) i.e., 6.4% loss in
515 EBC per day (similar removal of EBC during the total transportation path is assumed). On account of
516 intense BB is prevalent over SEA region during the springtime, it is possible that EBC aerosols get
517 coated with various organic aerosols and become hydrophilic in nature leading to hygroscopic
518 swelling and successive scavenging (e.g., Spackman et al., 2008; Girach et al., 2014). Nevertheless,
519 Chuang et al. (2016b) recently revealed the degradation of springtime (from March to April 2010 and
520 from February to April 2013) $PM_{2.5}$, EC, and anhydrosugars during the long-range atmospheric
521 transport from SEA source region to Mt. Lulin on the basis of estimated modification factors by
522 using non-sea-salt potassium ion (nss-K^+) and/or fractionalized EC evolved at 580 °C after pyrolized
523 organic carbon (OP) correction (EC1-OP) as the BB chemical tracers. However, the detailed and
524 more accurate role of EBC deposition can be better understood by analyzing the chemical transport

525 model and synoptic-scale meteorology in western Pacific region of East Asia.

526 **4. Summary**

527 Analyses of simultaneously measured EBC and CO concentrations at LABS at the summit of
528 Mt. Lulin, Taiwan from June 2012 to May 2014 along with BTs analysis, fire-counts data,
529 meteorological parameters, and emission ratios brought out some important outcomes. The major
530 findings from this study are:

531 • Clear monthly variation and the impact of long-range transport on the EBC and CO surface
532 concentrations were observed at LABS. Both EBC and CO concentrations displayed bimodal
533 distributions with the major mode in March and the less pronounced minor mode in October.
534 The minor peak in both EBC and CO during October was due to the influence of Asian
535 continental outflow from mainland China. However, the highest concentrations (mean ± 1σ;
536 median) of EBC (883 ± 621 ng m^{-3}; 840 ng m^{-3}) and CO (209 ± 71 ppbv; 212 ppbv) during
537 March were primarily attributed to the westerly winds coupled with BB emissions from SEA
538 region. In addition to the influence of long-range transported BB emissions from SEA and
539 China, these peak concentrations were found also be associated with low RH and rainfall.

540 • The annual median (mean ± 1σ) concentration of EBC and CO were found to be 117 ng m^{-3}
541 (275 ± 406 ng m^{-3}) and 129 ppbv (140 ± 52 ppbv), respectively at LABS. EBC and CO
542 showed similar seasonal variations with the highest in spring and the lowest in summer.

543 • The statistical correlation between EBC and CO was found to be good during February–
544 April, whereas it was poor for other months. This difference may be due to meteorological
545 processes (washout/rainout) or due to the mixing/dilution of air masses transported far from
546 the mainland to a high-altitude mountain environment like Mt. Lulin.

- The ΔEBC/ΔCO ratio at Mt. Lulin was found to be the highest during March (mean ± standard error at 95% confidence interval; 5.3 ± 0.3 ng m^{-3} $ppbv^{-1}$). However, on the basis of episodic cases, ΔEBC/ΔCO ratios were estimated to be 6.1 ± 0.7, 8.0 ± 2.1, and 2.4 ± 0.6 ng m^{-3} $ppbv^{-1}$ for SEA BB emissions, southern China mixed pollution, and northern China mixed pollution, respectively.
- A total of 32% loss in EBC aerosols (6.4% loss in EBC per day) was estimated for the atmospheric transport of BB emissions from SEA region to LABS.

The large differences in ΔEBC/ΔCO ratios seen at Mt. Lulin spotlight the need for more detailed studies on the EBC-CO relationship over Taiwan as well as other high-mountain remote sites in East Asia. This study at a high altitude background station in East Asia will be immensely helpful to validate the bottom-up emission inventories as well as in reduction of associated uncertainties in aerosol modelling simulation over the region. Moreover, the estimated ΔEBC/ΔCO ratios at Mt. Lulin would be used in model simulations to evaluate the BC aging and scavenging over the western Pacific region in East Asia.

Conflicts of interest

The authors declare that there is no conflict of interests regarding financial funding and the publication of this paper.

Acknowledgments

We express our thanks to all assistants involved in the system installation, maintenance, and site operation at Mt. Lulin station. S. K. Pani sincerely thanks to the Ministry of Science and Technology, Taiwan being a receiver of Post-Doctoral Fellowship (Project Number, MOST 106-2811-M-008-032 and 107-2811-M-008-2527). The authors gratefully acknowledge the NOAA Air

569 Resources Laboratory (ARL) for the provision of HYSPLIT model and/or READY website
570 (http://www.arl.noaa.gov/ready.php) used in this manuscript. CALIPSO lidar images were obtained
571 from the web page of https://www-calipso.larc.nasa.gov. The deployment of NASA Surface-based
572 Mobile Atmospheric Research and Testbed Laboratories (SMARTLabs;
573 https://smartlabs.gsfc.nasa.gov/) at Doi Ang Khang in northern Thailand during 7-SEAS/BASELInE
574 (http://rsm2.atm.ncu.edu.tw/) 2013 campaign was partially supported by NASA Radiation Sciences
575 Program and managed by Dr. Hal B. Maring and Dr. Si-Chee Tsay. The authors would like to thank
576 the Editor and three anonymous reviewers for their critical and useful comments, which significantly
577 improved the quality of the manuscript.

578 **References**

579 Andreae, M.O., Schmid, O., Yang, H., Chanda, D., Yu, J.Z., Zeng, L.M., Zhang, Y.H., 2008. Optical
580 properties and chemical composition of the atmospheric aerosol in urban Guangzhou, China.
581 Atmos. Environ. 42, 6335–6350.

582 Andrews, E., Ogren, J.A., Bonasoni, P., Marinoni, A., Cuevas, E., Rodríguez, S., Sun, J.Y., Jaffe,
583 D.A., Fischer, E.V., Baltensperger, U., Weingartner, E., Collaud Coen, M., Sharma, S.,
584 Macdonald, A.M., Leaitch,W.R., Lin, N.H., Laj, P., Arsov, T., Kalapov, I., Jefferson, A.,
585 Sheridan, P., 2011. Climatology of aerosol radiative properties in the free troposphere. Atmos.
586 Res. 102, 365–393.

587 Andrews, E., Sheridan, P.J., Ogren, J.A., Hageman, D., Jefferson, A., Wendell, J., Alados-Arboledas,
588 L., Bergin, M., Ealo, M., Hallar, A.G., Hoffer, A., Kalapov, I., Kim, J., Kim, S.W., Kolonjari, F.,
589 Labuschagne, C., Leaitch, R., Lin, N.H., Macdonald, A.M., Mayol-Bracero, O.L., Pondolfi, M.,
590 Sharma, S., Sherman, J.P., Sorribas, M., Sun, J., 2019. Overview of the NOAA/ESRL Federated
591 Aerosol Network. Bull. Amer. Meteor. Soc. 100, 123–135.

592 Babu, S.S., Chaubey, J.P., Moorthy, K.K., Gogoi, M.M., Kompalli, S.K., Sreekanth, V., Bagare, S.P.,
593 Bhatt, B.C., Gaur, V.K., Prabhu, T.P., Singh, N.S., 2011. High altitude (~4520 m amsl)
594 measurements of black carbon aerosols over western trans-Himalayas: Seasonal heterogeneity
595 and source apportionment. J. Geophys. Res. 116, D24201.

596 Backman, J., Schmeisser, L., Virkkula, A., Ogren, J. A., Asmi, E., Starkweather, S., Sharma, S.,
597 Eleftheriadis, K., Uttal, T., Jefferson, A., Bergin, M., Makshtas, A., Tunved, P., Fiebig, M., 2017.
598 On Aethalometer measurement uncertainties and an instrument correction factor for the Arctic.

599 Atmos. Meas. Tech. 10, 5039–5062.

600 Baumgardner, D., Raga, G., Peralta, O., Rosas, I., Castro, T., Kuhlbusch, T., John, A., Petzold, A.,
601 2002. Diagnosing black carbon trends in large urban areas using carbon monoxide
602 measurements, J. Geophys. Res. 107 (D21), 8342.

603 Bodhaine, B.A., 1995. Aerosol absorption measurements a Barrow, Mauna Loa and the south pole. J.
604 Geophys. Res. 100 (D5), 8967–8975.

605 Bond, T.C., Bergstrom, R.W., 2006. Light absorption by carbonaceous particles, an investigative
606 review. Aerosol Sci. Technol. 40, 27–67.

607 Bond, T.C., Streets, D.G., Yarber, K.F., Nelson, S.M., Woo, J.H., Klimont, Z., 2004. A technology-
608 based global inventory of black and organic carbon emissions from combustion. J. Geophys.
609 Res. 109, D14203.

610 Bond, T.C., Doherty, S.J., Fahey, D.W., Forster, P.M., Berntsen, T., DeAngelo, B.J., Flanner, M.G.,
611 Ghan, S., Karcher, B., Koch, D., Kinne, S., Kondo, Y., Quinn, P.K., Sarofim, M.C., Schultz,
612 M.G., Schulz, M., Venkataraman, C., Zhang, H., Zhang, S., Bellouin, N., Guttikunda, S.K.,
613 Hopke, P.K., Jacobson, M.Z., Kaiser, J.W., Klimont, Z., Lohmann, U., Schwarz, J.P., Shindell,
614 D., Storelvmo, T., Warren, S.G., Zender, C.S., 2013. Bounding the role of black carbon in the
615 climate system, A scientific assessment. J. Geophys. Res. Atmos. 118, 5380–5552.

616 Cao, J., Tie, X., Xu, B., Zhao, Z., Zhu, C., Li, G., Liu, S., 2010. Measuring and modeling black
617 carbon (BC) contamination in the SE Tibetan Plateau. J. Atmos. Chem. 67, 45–60.

618 Cape, J.N., Coyle, M., Dumitrean, P., 2012. The atmospheric lifetime of black carbon. Atmos.
619 Environ. 59, 256–263.

620 Chen, L.W.A., Doddridge, B.G., Dickerson, R.R., Chow, J.C., Mueller, P.K., Quinn, J., Butler, W.A.,
621 2001. Seasonal variations in elemental carbon aerosol, carbon monoxide and sulfur dioxide,
622 implications for sources. Geophys. Res. Lett. 28 (9), 1711–1714.

623 Chen, J., Li, C., Ristovski, Z., Milic, A., Gu, Y., Islam, M.S., Wang, S., Hao, J., Zhang, H., He, C.,
624 Guo, H., Fu, H., Miljevic, B., Morawska, L., Thai, P., Lam, Y.F., Pereira, G., Ding, A., Huang,
625 X., Dumka, U.C., 2017. A review of biomass burning, emissions and impacts on air quality,
626 health and climate in China. Sci. Total Environ. 579, 1000–1034.

627 Chou, C.C.K., Lee, C.T., Cheng, M.T., Yuan, C.S., Chen, S.J., Wu, Y.L., Hsu, W.C., Lung, S.C., Hsu,
628 S.C., Lin, C.Y., Liu, S.C., 2010. Seasonal variation and spatial distribution of carbonaceous
629 aerosols in Taiwan. Atmos. Chem. Phys. 10, 9563–9578.

630 Chuang, M.T., Lee, C.T., Lin, N.H., Chou, C.C.K., Wang, J.L., Sheu, G.R., Chang, S.C., Wang, S.H.,
631 Huang, H., Cheng, H.W., Weng, G.H., Lai, S.Y., Hsu, S.P., Chang, Y.J., 2014. Carbonaceous

aerosols in the air masses transported from Indochina to Taiwan, Long-term observation at Mt. Lulin. Atmos. Environ. 89, 507–516.

Chuang, M.T., Fu, J.S., Lee, C.T., Lin, N.H., Gao, Y., Wang, S.H., Sheu, G.R., Hsiao, T.C., Wang, J.L., Yen, M.C., Lin, T.H., Thongboonchoo, N., 2016a. The simulation of long-range transport of biomass burning plume and short-range transport of anthropogenic pollutants to a mountain observatory in East Asia during the 7-SEAS/2010 Dongsha Experiment. Aerosol Air Qual. Res. 16, 2933–2949.

Chuang, M.T, Lee, C.T, Chou, C.C.K., Engling, G., Chang, S.Y., Chang, S.C., Sheu, G.R., Lin, N.H., Sopajaree, K., Chang, Y.J., Hong, G.J., 2016b. Aerosol transport from Chiang Mai, Thailand to Mt. Lulin, Taiwan – Implication of aerosol aging during long-range transport. Atmos. Environ. 137, 101–112.

Chuang, M.T., Chou, C.C.K., Lin, N.H., Takami, A., Hsiao, T.C., Lin, T.H., Fu, J.S., Pani, S.K., Lu, Y.R., Yang, T.Y., 2017. A simulation study on $PM_{2.5}$ sources and meteorological characteristics at the northern tip of Taiwan in the early stage of the Asian haze period. Aerosol Air Qual. Res. 17, 3166–3178.

Chung, C.E., Ramanathan, V., Kim, D., Podgorny, I., 2005. Global anthropogenic aerosol direct forcing derived from satellite and ground-based observations. J. Geophys. Res. 110, D24207.

Chung, C.E., Ramanathan, V., Carmichael, G., Kulkarni, S., Tang, Y., Adhikary, B., Leung, L. R., Qian, Y., 2010. Anthropogenic aerosol radiative forcing in Asia derived from regional models with atmospheric and aerosol data assimilation. Atmos. Chem. Phys. 10, 6007–6024.

Collaud Coen, M.,Weingartner, E.,Apituley, A., Ceburnis,D., Fierz-Schmidhauser, R., Flentje, H., Henzing, J.S., Jennings, S.G.,Moerman,M., Petzold, A., Schmid, O., Baltensperger, U., 2010. Minimizing light absorption measurement artifacts of the Aethalometer, evaluation of five correction algorithms. Atmos. Meas. Tech. 3, 457–474.

Conant, W.C., Nenes, A., Seinfeld, J.H., 2002. Black carbon radiative heating effects on cloud microphysics and implications for aerosol indirect effect 1. Extended Köhler theory, J. Geophys. Res., 107(D21), 4604.

Corrigan, C.E., Ramanathan, V., Schauer, J.J., 2006. Impact of monsoon transitions on the physical and optical properties of aerosols. J. Geophys. Res. 111, D18208.

Cristofanelli, P., Bracci, A., Sprenger, M., Marinoni, A., Bonafè, U., Calzolari, F., Duchi, R., Laj, P., Pichon, J. M., Roccato, F., Venzac, H., Vuillermoz, E., Bonasoni, P., 2010. Tropospheric ozone variations at the Nepal Climate Observatory- Pyramid (Himalayas, 5079 m a,s,l,) and influence of deep stratospheric intrusion events. Atmos. Chem. Phys. 10, 6537–6549.

Deeter, M.N., Edwards, D.P., Gille, J.C., Drummond, J.R., 2009. CO retrievals based on MOPITT

near-infrared observations. J. Geophys. Res. Atmos. 114, D04303.

Delene, D.J., Ogren, J.A., 2002. Variability of aerosol optical properties at four North American surface monitoring sites. J. Atmos. Sci. 59, 1135–1150.

Derwent, R.G., Ryall, D.B., Jennings, S.G., Spain, T.G., Simmonds, P.G., 2001. Black carbon aerosol and carbon monoxide in European regionally polluted air masses at Mace Head, Ireland during 1995–1998. Atmos. Environ. 35(36), 6371–6378.

Dickerson, R.R., Andreae, M.O., Campos, T., Mayol-Bracero, O.L., Neususess, C., Streets, D.G., 2002. Analysis of black carbon and carbon monoxide observed over the Indian Ocean, implications for emissions and photochemistry. J. Geophys. Res. 107 (D19), 8017.

Draxler, R.R., Rolph, G.D., 2013. HYSPLIT (Hybrid Single-Particle Lagrangian Integrated Trajectory) Model Access via NOAA ARL READY Website, (http,//www. arl.noaa.gov/HYSPLIT.php), NOAA Air Resources Laboratory, College Park, MD.

Dumka, U.C., Moorthy, K.K, Kumar, R., Hegde, P., Sagar, R., Pant, P., Singh, N., Babu, S.S., 2010. Characteristics of Aerosol Black Carbon Mass Concentration over a High Altitude Location in the Central Himalayas from Multi-year Measurements. Atmos. Res. 96, 510–521.

Duncan, B.N., Logan, J.A., Bey, I., Megretskaia, I.A., Yantosca, R.M., Novelli, P.C., Jones, N.B., Rinsland, C.P., 2007. Global budget of CO, 1988-1997, source estimates and validation with a global model. J. Geophys. Res. 112, D22301.

Engling, G., Zhang, Y.N., Chan, C.Y., Sang, X.F., Lin, M., Ho, K.F., Li, Y.S., Lin, C.Y., Lee, J.J., 2011. Characterization and sources of aerosol particles over the southeastern Tibetan Plateau during the Southeast Asia biomass-burning season. Tellus B, Chemical and Physical Meteorology 63 (1), 117–128.

Engström, J.E., Leck, C., 2017. Seasonal variability in atmospheric black carbon at three stations in South-Asia. Tellus B, Chemical and Physical Meteorology 69 (1), 1131102.

Finlayson-Pitts, B.J., Pitts Jr., J.N., 2000. Chemistry of the Upper and Lower Atmosphere, Theory, Experiments, and Applications. Academic, London.

Forster, P., Ramaswamy, V., Artaxo, P., Berntsen, T., Betts, R.A., Fahey, D.W., Haywood, J., Lean, J., Lowe, D.C., Myhre, G., Nganga, J., Prinn, R., Raga, G., Schulz, M., Van Dorland, R., 2007. Changes in Atmospheric Constituents and Radiative Forcing. Chapter 2 of the Climate Change 2007, The Physical Science Basis, IPCC – Intergovernmental Panel on Climate Change Book. Cambridge University Press, United Kingdom, ISSN 978-0-521-88009-1.

Freney, E., Karine, S., Eija, A., Clemence, R., Aurelien, C., Jean-Luc, B., Aurelie, C., Maxime, H., Nadege, M., Laeticia, B., David, P., 2016. Experimental Evidence of the Feeding of the Free

Troposphere with Aerosol Particles from the Mixing Layer. Aerosol Air Qual. Res. 16, 702–716.

Girach, I., Nair, V., Babu, S., Nair, P., 2014. Black carbon and carbon monoxide over Bay of Bengal during W_ICARB: Source characteristics. Atmos. Environ. 94, 508–517.

Guo, Q., Hu, M., Guo, S., Wu, Z., Peng, J., Wu, Y., 2017. The variability in the relationship between black carbon and carbon monoxide over the eastern coast of China, BC aging during transport. Atmos. Chem. Phys. 17, 10395–10403.

Han, S., Kondo, Y., Oshima, N., Takegawa, N., Miyazaki, Y., Hu, M., Lin, P., Deng, Z., Zhao, Y., Sugimoto, N., Wu, Y., 2009. Temporal variations of elemental carbon in Beijing. J. Geophys. Res. 114(D23), D23202.

Hansen, A.D.A., 2005. The Aethalometer, Manual. Magee Scientific, Berkeley, California, USA.

Hansen, A.D.A., Rosen, H., Novakov, T., 1984. The aethalometer, an instrument for the realtime measurements of optical absorption by aerosol particles, Sci. Total Environ. 36, 191–196.

Haywood, J.M., Boucher, O., 2000. Estimates of the direct and indirect radiative forcing due to tropospheric aerosols, A review. Rev. Geophys. 38, 513–543.

Hsiao, T.C., Ye, W.C., Wang, S.H., Tsay, S.C., Chen, W.N., Lin, N.H., Lee, C.T., Hung, H.M., Chuang, M.T., Chantara, S., 2016. Investigation of the CCN activity, BC and UVBC mass concentrations of biomass burning aerosols during the 2013 BASELInE campaign. Aerosol Air Qual. Res. 16, 2742–2756.

Hsiao, T.C., Chen, W.N., Ye, W.C., Lin, N.H., Tsay, S.C., Lin, T.H., Lee, C.T., Chuang, M.T., Pantina, P., Wang, S.H., 2017. Aerosol optical properties at the Lulin Atmospheric Background Station in Taiwan and the influences of long-range transport of air pollutants. Atmos. Environ. 150, 366–378.

Hyvärinen, A.P., Lihavainen, H., Komppula, M., Sharma, V.P., Kerminen, V.M., Panwar, T.S., Viisanen, Y., 2009. Continuous measurements of optical properties of atmospheric aerosols in Mukteshwar, northern India. J. Geophys. Res. 114, D08207.

IPCC, 2007. Climate Change 2007: Contribution of Working Group III to the Fourth Assessment Report of the Intergovernmental Panel on Climate Change, Metz, B., Davidson, O.R., Bosch, P.R., Dave, R. and Meyer, L.A. (Eds.), Cambridge University Press, Cambridge, United Kingdom and New York, NY, USA.

IPCC, 2013. Climate Change 2013: The Physical Science Basis, Report of Working Group I to the Fifth Assessment of the IPCC. Cambridge University Press, Cambridge, United Kingdom and New York, NY, USA.

731 Jacobson, M.Z., 2001. Strong radiative heating due to the mixing state of black carbon in
732 atmospheric aerosols. Nature 409 (6821), 695–697.

733 Jaffe, D.A., Sedlacek, A., Laing, J.R., 2017. Black Carbon at the Mt. Bachelor Observatory Field
734 Campaign Report. United States.

735 Jefferson, A., 2011. Aerosol Observing System (AOS) handbook, Tech. Rep. ARM-TR-014, U.S.
736 Dep. of Energy, Washington, D. C.

737 Jennings, S.G., Spain, T.G., Doddridge, B.G., Maring, H., Kelly, B.P., Hansen, A.D.A., 1996.
738 Concurrent measurements of black carbon aerosol and carbon monoxide at Mace Head. J.
739 Geophys. Res. 101, 19447–19454.

740 Kanaya, Y., Pan, X., Miyakawa, T., Komazaki, Y., Taketani, F., Uno, I., Kondo, Y., 2016. Long-term
741 observations of black carbon mass concentrations at Fukue Island, western Japan, during 2009–
742 2015, constraining wet removal rates and emission strengths from East Asia. Atmos. Chem.
743 Phys. 16, 10689–10705.

744 Khamkaew, C., Chantara, S., Janta, R., Pani, S.K., Prapamontol, T., Kawichai, S., Wiriya, W., Lin,
745 N.H., 2016. Investigation of biomass burning chemical components over northern Southeast Asia
746 during 7-SEAS/BASELInE 2014 campaign. Aerosol Air Qual. Res. 16, 2655–2670.

747 Kim, H.S., Tans, P.P., Novelli, P.C., 2008. On the regional background levels of carbon monoxide
748 observed in East Asia during 1991 similar to 2004. Air Quality, Atmosphere & Health 1, 37–44.

749 Kirchstetter, T.W., Novakov, T., 2007. Controlled generation of black carbon particles from a
750 diffusion flame and applications in evaluating black carbon measurement methods. Atmos.
751 Environ. 41, 1874–1888.

752 Kondo, Y., Komazaki, Y., Miyazaki, Y., Moteki, N., Takegawa, N., Kodama, D., Deguchi, S.,
753 Nogami, M., Fukuda, M., Miyakawa, T., 2006. Temporal variations of elemental carbon in
754 Tokyo. J. Geophys. Res. 111, D12205.

755 Lack, D.A., Langridge, J.M., Bahreini, R., Cappa, C.D., Middlebrook, A.M., Schwarz, J.P., 2012.
756 Brown carbon and internal mixing in biomass burning particles. Proc. Natl. Acad. Sci. 109,
757 14802–14807.

758 Lee, C.T., Chuang, M.T., Lin, N.H., Wang, J.L., Sheu, G.R., Wang, S.H., Huang, H., Chen, H.W.,
759 Weng, G.H., Hsu, S.P., 2011. The enhancement of $PM_{2.5}$ mass and water-soluble ions of
760 biosmoke transported from Southeast Asia over the Mountain Lulin site in Taiwan. Atmos.
761 Environ. 45, 5784–5794.

762 Lin, N.H., Tsay, S.C., Reid, J.S., Yen, M.C., Sheu, G.R.,Wang, S.H., Chi, K.H., Chuang, M.T., Ou-
763 Yang, C.F., Fu, J.S., Lee, C.T., Wang, L.C., Wang, J.L., Hsu, C.N., Holben, B.N., Chu, Y.C.,

764 Maring, H.B., Nguyen, A.X., Sopajaree, K., Chen, S.J., Cheng, M.T., Tsuang, B.J., Tsai, C. J.,
765 Peng, C.M., Chang, C.T., Lin, K.S., Tsai, Y.I., Lee, W.J., Chang, S.C., Liu, J.J., Chiang, W. L.
766 2013. An overview of regional experiments on biomass burning aerosols and related pollutants in
767 Southeast Asia, from BASE-ASIA and Dongsha Experiment to 7-SEAS. Atmos. Environ. 78, 1–
768 19.

769 Lin, N.H., Sayer, A.M., Wang, S.H., Loftus, A.M., Hsiao, T.C., Sheu, G.R., Hsu, N.C., Tsay, S.C.,
770 Chantara, S., 2014. Interactions between biomass-burning aerosols and clouds over Southeast
771 Asia, Current status, challenges, and perspectives. Environ. Pollut. 195, 292–307.

772 Liousse, C., Cachier, H., Jennings, S.G., 1993. Optical and thermal measurements of black carbon
773 aerosol content in different environments, Variation of specific attenuation cross section, sigma
774 (σ). Atmos. Environ. 27(A), 1203-1211.

775 Liu, J., Fan, S., Horowitz, L.W., Levy, H., 2011. Evaluation of factors controlling long-range
776 transport of black carbon to the arctic. J. Geophys. Res. 116, D04307.

777 Logan, J.A., Prather, M.J., Wofsy, S.C., McElroy, M.B., 1981. Tropospheric chemistry, a global
778 perspective. J. Geophys. Res. 86, 7210–7254.

779 Ma, J.Z., Tang, J., Li, S.M., Jacobson, M.Z., 2003. Size distributions of ionic aerosols measured at
780 Waliguan Observatory, implication for nitrate gas-to-particle transfer processes in the free
781 troposphere. J. Geophys. Res. 108(D17), 4541.

782 Marinoni, A., Cristofanelli, P., Laj, P., Duchi, R., Calzolari, F., Decesari, S., Sellegri, K., Vuillermoz,
783 E., Verza, G. P., Villani, P., Bonasoni, P., 2010. Aerosol mass and black carbon concentrations, a
784 two year record at NCO-P (5079 m, Southern Himalayas). Atmos. Chem. Phys. 10, 8551–8562.

785 McClure, C.D., Jaffe, D.A., Gao, H., 2016. Carbon Dioxide in the Free Troposphere and Boundary
786 Layer at the Mt. Bachelor Observatory. Aerosol Air Qual. Res. 16, 717–728.

787 McMeeking, G.R., Hamburger, T., Liu, D., Flynn, M., Morgan, W.T., Northway, M., Highwood, E.J.,
788 Krejci, R., Allan, J.D., Minikin, A., Coe, H., 2010. Black carbon measurements in the boundary
789 layer over western and northern Europe. Atmos. Chem. Phys. 10, 9393–9414.

790 Miguel, A.H., Kirchstetter, T.W., Harley, R.A., 1998. On-road emissions of particulate polycyclic
791 aromatic hydrocarbons and black carbon from gasoline and diesel vehicles. Environ. Sci.
792 Technol. 32, 450–455.

793 Moorthy, K.K., Babu, S.S., Sunilkumar, S.V., Gupta, P.K., Gera, B.S., 2004. Altitude profiles of
794 aerosol BC, derived from aircraft measurements over an inland urban location in India. Geophys.
795 Res. Lett. 31, L22103.

796 Narita, D., Pochanart, P., Matsumoto, J., Someno, K., Tanimoto, H., Hirokawa, J., Kajii, Y., Akimoto,

H., Nakao, M., Katsuno, T., Kinjo, Y., 1999. Seasonal variation of carbon monoxide at remote sites in Japan. Chemosphere - Global Change Science 1 (1–3), 137–144.

Okamoto, S., Tanimoto, H., 2016. A review of atmospheric chemistry observations at mountain sites. Progress in Earth and Planetary Science 3, 34.

Oltmans, S.J., Komhyr, W.D., 1986. Surface ozone distributions and variations from 1973 to 1984 measurements at the NOAA geophysical monitoring for climatic change baseline observatories. J. Geophys. Res. 91, 5229–5236.

Oshima, N., Kondo, Y., Moteki, N., Takegawa, N., Koike, M., Kita, K., Matsui, H., Kajino, M., Nakamura, H., Jung, J.S., Kim, Y.J., 2012. Wet removal of black carbon in Asian outflow, Aerosol Radiative Forcing in East Asia (A-FORCE) aircraft campaign. J. Geophys. Res. 117, D03204.

Ou-Yang, C.F., Chang, C.C., Wang, J.L., Shimada, K., Hatakeyama, S., Kato, S., Chiu, J.Y., Sheu, G.R., Lin, N.H., 2017. Characteristics of Summertime Volatile Organic Compounds in the Lower Free Troposphere, Background Measurements at Mt. Fuji. Aerosol Air Qual. Res. 17, 3037–3051.

Ou-Yang, C.F., Lin, N.H., Lin, C.C., Wang, S.H., Sheu, G.R., Lee, C.T., Schnell, R.C., Lang, P.M., Kawasato, T., Wang, J.L., 2014. Characteristics of atmospheric carbon monoxide at a high-mountain background station in East Asia. Atmos. Environ. 89, 613–622.

Ou-Yang, C.F., Lin, N.H., Sheu, G.R., Lee, C.T., Wang, J.L., 2012. Seasonal and diurnal variations of ozone at a high-altitude mountain baseline station in East Asia. Atmos. Environ. 46, 279–288.

Pan, X.L., Kanaya, Y., Wang, Z.F., Liu, Y., Pochanart, P., Akimoto, H., Sun, Y.L., Dong, H.B., Li, J., Irie, H., Takigawa, M., 2011. Correlation of black carbon aerosol and carbon monoxide in the high-altitude environment of Mt. Huang in Eastern China. Atmos. Chem. Phys. 11, 9735–9747.

Pani, S.K., 2013. Sources and Radiative Effects of Ambient Aerosols in an Urban Atmosphere in East India. Ph. D. Thesis. Indian Institute of Technology Kharagpur, India.

Pani, S.K., Verma, S., 2014. Variability of winter and summertime aerosols over eastern India urban environment. Atmos. Res. 137, 112–124.

Pani, S.K., Wang, S.H., Lin, N.H., Tsay, S.C., Lolli, S., Chuang, M.T., Lee, C.T., Chantara, S., Yu, J.Y. 2016a. Assessment of aerosol optical property and radiative effect for the layer decoupling cases over the Northern South China Sea during the 7-SEAS/Dongsha Experiment. J. Geophys. Res. Atmos. 121, 4894–4906.

Pani, S.K., Wang, S.H., Lin, N.H., Lee, C.T., Tsay, S.C., Holben, B.N., Janjai, S., Hsiao, T.C., Chuang, M.T., Chantara, S., 2016b. Radiative effect of springtime biomass-burning aerosols over

Northern Indochina during 7-SEAS/BASELInE 2013 campaign. Aerosol Air Qual. Res. 16, 2802–2817.

Pani, S.K., Wang, S.H., Lin, N.H., Lee, C.T., Tsay, S.C., Holben, B.N., Janjai, S., Hsiao, T.C., Chuang, M.T., Chantara, S., 2016c. Impact of Springtime Biomass-Burning Aerosols on Radiative Forcing over Northern Thailand during the 7-SEAS Campaign. In: European Geophysical Union General Assembly, 18, EGU2016-11795.

Pani, S.K., Lee, C.T., Chou, C.C.K., Shimada, K., Hatakeyama, S., Takami, A., Wang, S.H., Lin, N.H., 2017. Chemical characterization of wintertime aerosols over islands and mountains in East Asia, impacts of the continental Asian outflow, Aerosol and Air Quality Research, 17 (12), 3006–3036.

Pani, S.K., Lin, N.H., Chantara, S., Wang, S.H., Khamkaew, C., Prapamontol, T., Janjai, S., 2018. Radiative response of biomass-burning aerosols over an urban atmosphere in northern peninsular Southeast Asia. Sci. Total Environ. 633, 892–911.

Pani, S.K., Chantara, S., Khamkaew, C., Lee, C.T., Lin, N.H., 2019. Biomass burning in the northern peninsular Southeast Asia: Aerosol chemical profile and potential exposure. Atmos. Res. 224, 180–195.

Park, R.J., Jacob, D.J., Paul, I.P., Clarke, A.D., Weber, R.J., Zondlo, M.A., Eisele, F.L., Bandy, A.R., Thornton, D.C., Sachse, G.W., Bond, T.C., 2005. Export efficiency of black carbon aerosol in continental outflow: global implications. J. Geophys. Res. Atmos. 110, D11205.

Park, S., Kim, S.W., Lin, N.H., Pani, S.K., Sheridan, P.J., Andrews, E., Shim, K., 2018. Variability of Aerosol Optical Properties in the Asian Continental Outflow Region: Marine background site (Gosan, Korea) vs. high-altitude mountain site (Lulin, Taiwan). In: American Geophysical Union, Fall Meeting, A21G–2760.

Park, S., Kim, S.W., Lin, N.H., Pani, S.K., Sheridan, P.J., Andrews, E., 2019. Variability of Aerosol Optical Properties Observed at Polluted Marine (Gosan, Korea) and high-altitude mountain (Lulin, Taiwan) sites in the Asian Continental Outflow. Aerosol and Air Qual. Res. https://doi.org/10.4209/aaqr.2018.11.0416.

Petzold, A., Kopp, C., Niessner, R., 1997. The dependence of the specific attenuation cross-section on black carbon mass fraction and particle size. Atmos. Environ. 31, 661–672.

Petzold, A., Ogren, J.A., Fiebig, M., Laj, P., Li, S.M., Baltensperger, U., Holzer-Popp, T., Kinne, S., Pappalardo, G., Sugimoto, N., Wehrli, C., Wiedensohler, A., Zhang, X.Y., 2013. Recommendations for reporting “black carbon” measurements. Atmos. Chem. Phys. 13, 8365–8379.

Pochanart, P., Akimoto, H., Kajii, Y., Potemkin, V.M., Khodzher, T.V., 2003. Regional background ozone and carbon monoxide variations in remote Siberia/East Asia. J. Geophys. Res. Atmos. 108

(D1), 4028.

Prather, M.J., 1996. Time scales in atmospheric chemistry, theory, GWPs for CH_4 and CO, and runaway growth. Geophys. Res. Lett. 23, 2597–2600.

Raju, M.P., Safai, P.D., Rao, P.S.P., Devara, P.C.S., Budhavant, K.B., 2011. Seasonal characteristics of black carbon aerosols over a high altitude station in Southwest India. Atmos. Res. 100, 103–110.

Ramanathan, V., Carmichael, G., 2008. Global and regional climate changes due to black carbon. Nature Geoscience 1, 221–227.

Reidmiller, D.R., Jaffe, D.A., Chand, D., Strode, S., Swartzendruber, P., Wolfe, G.M., Thornton, J.A., 2009. Interannual variability of long-range transport as seen at the Mt. Bachelor Observatory. Atmos. Chem. Phys. 9, 557–572.

Sahu, L.K., Kondo, Y., Miyazaki, Y., Kuwata, M., Koike, M., Takegawa, N., Tanimoto, H., Matsueda, H., Yoon, S.C., Kim, Y.J., 2009. Anthropogenic aerosols observed in Asian continental outflow at Jeju Island, Korea, in spring 2005. J. Geophys. Res. 114, D03301.

Sarkar, C., Chatterjee, A., Singh, A.K., Ghosh, S.K., Raha, S., 2015. Characterization of Black Carbon Aerosols over Darjeeling - A High Altitude Himalayan Station in Eastern India. Aerosol and Air Qua. Res. 15, 465–478.

Sharma, S., Leaitch, W.R., Huang, L., Veber, D., Kolonjari, F., Zhang, W., Hanna, S.J., Bertram, A.K., Ogren, J.A., 2017. An evaluation of three methods for measuring black carbon in Alert, Canada. Atmos. Chem. Phys. 17, 15225–15243.

Sherman, J.P., Sheridan, P.J., Ogren, J.A., Andrews, E., Hageman, D., Schmeisser, L., Jefferson, A., Sharma, S., 2015. A multi-year study of lower tropospheric aerosol variability and systematic relationships from four North American regions. Atmos. Chem. Phys. 15, 12487–12517.

Shen, X., Sun, J., Zhang, X., Kivekäs, N., Zhang, Y., Wang, T., Zhang, X., Yang, Y., Wang, D., Zhao, Y., Qin, D., 2016. Particle Climatology in Central East China Retrieved from Measurements in Planetary Boundary Layer and in Free Troposphere at a 1500-m-High Mountaintop Site. Aerosol Air Qual. Res. 16, 689–701.

Sheridan, P.J., Arnott, W.P., Ogren, J.A., Andrews, E., Atkinson, D.B., Covert, D.S., Moosmuller, H., Petzold, A., Schmid, B., Strawa, A.W., Varma, R., Virkkula, A., 2005. The Reno Aerosol Optics Study, An Evaluation of Aerosol Absorption Measurement Methods. Aerosol Sci. Technol. 39, 1–16.

Sheridan, P.J., Delene, D.J., Ogren, J.A., 2001. Four years of continuous surface aerosol measurements from the department of energy's atmospheric radiation measurement program

southern great plains cloud and radiation testbed site. J. Geophys. Res. Atmos. 106, 20735–20747.

Sheu, G.R., Lin, N.H., Wang, J.L., Lee, C.T., Ou-Yang, C.F., Wang, S.H., 2010. Temporal distribution and potential sources of atmospheric mercury measured at a high-elevation background station in Taiwan. Atmos. Environ. 44, 2393–2400.

Sikder, H.A., Suthawaree, J., Kato, S., Kajii, Y., 2011. Surface ozone and carbon monoxide levels observed at Oki, Japan, regional air pollution trends in East Asia. J. Environ. Management 92, 953–959.

Spackman, J.R., Schwarz, J.P., Gao, R.S., Watts, L.A., Thomson, D.S., Fahey, D.W., Holloway, J.S., de Gouw, J.A., Trainer, M., Ryerson, T.B., 2008. Empirical correlations between black carbon aerosol and carbon monoxide in the lower and middle troposphere. Geophys. Res. Lett. 35(19), L19816.

Subramanian, R., Kok, G.L., Baumgardner, D., Clarke, A., Shinozuka, Y., Campos, T.L., Heizer, C.G., Stephens, B.B., de Foy, B., Voss, P.B., Zaveri, R.A., 2010. Black carbon over Mexico, the effect of atmospheric transport on mixing state, mass absorption cross-section, and BC/CO ratios. Atmos. Chem. Phys. 10, 219–237.

Suthawaree, J., Kato, S., Takami, A., Kadena, H., Toguchi, M., Yogi, K., Hatakeyama, S., Kajii, Y. 2008. Observation of ozone and carbon monoxide at Cape Hedo, Japan, seasonal variation and influence of long-range transport. Atmos. Environ. 42, 2971–2981.

Tang, Y.H., Carmichael, G.R., Woo, J.H., Thongboonchoo, N., Kurata, G., Uno, I., Streets, D.G., Blake, D.R., Weber, R.J., Talbot, R.W., Kondo, Y., Singh, H.B., Wang, T., 2003. Influences of biomass burning during the transport and chemical evolution over the Pacific (TRACE-P) experiment identified by the regional chemical transport model. J. Geophys. Res. 108 (D21), 8824.

Thompson, A.M., Cicerone, R.J., 1986. Possible perturbations to atmospheric CO, CH_4, and OH. J. Geophys. Res. 91, 10853–10864.

Thompson, A.M., 1992. The oxidizing capacity of the earth's atmosphere: probable past and future changes. Science 256, 1157–1165.

Tsay, S.C., Maring, H.B., Lin, N.H., Buntoung, S., Chantara, S., Chuang, H.C., Gabriel, P.M., Goodloe, C.S., Holben, B.N., Hsiao, T.C., Hsu, N.C., Janjai, S., Lau, W.K.M., Lee, C.T., Lee, J., Loftus, A.M., Nguyen, A.X., Nguyen, C.M., Pani, S.K., Pantina, P., Sayer, A.M., Tao, W.K., Wang, S.H., Welton, E.J., Wiriya, W., Yen, M.C., 2016. Satellite-surface perspectives of air quality and aerosol-cloud effects on the environment: An overview of 7-SEAS/BASELInE. Aerosol Air Qual. Res. 16, 2581–2602.

931 Tsutsumi, Y., Mori, K., Ikegami, M., Tashiro, T., Tsuboi, K., 2006. Long-term trends of greenhouse
932 gases in regional and background events observed during 1998–2004 at Yonagunijima located to
933 the east of the Asian continent. Atmos. Environ. 40, 5868–5879.

934 Udayasoorian, C., Jayabalakrishnan, R.M., Suguna, A.R., Gogoi, M.M., Babu, S.S., 2014. Aerosol
935 black carbon characteristics over a high-altitude Western Ghats location in Southern India. Ann.
936 Geophys. 32, 1361–1371.

937 Verma, R.L., Sahu, L.K., Kondo, Y., Takegawa, N., Han, S., Jung, J.S., Kim, Y.J., Fan, S., Sugimoto,
938 N., Shammaa, M.H., Zhang, Y.H., Zhao, Y., 2010. Temporal variations of black carbonin
939 Guangzhou, China, in summer 2006, Atmos. Chem. Phys. 10, 6471–6485.

940 Verma, R.L., Kondo, Y., Oshima, N., Matsui, H., Kita, K., Sahu, L.K., Kato, S., Kajii, Y., Takami, A.,
941 Miyakawa, T., 2011. Seasonal variations of the transport of black carbon and carbon monoxide
942 from the Asian continent to the western Pacific in the boundary layer. J. Geophys. Res. 116,
943 D21307.

944 Verma, S., Pani, S.K., Bhanja, S.N., 2013. Sources and radiative effects of wintertime black carbon
945 aerosols in an urban atmosphere in East India. Chemosphere 90, 260–269.

946 Verma, S., Bhanja, S.N., Pani, S.K., Misra, A., 2014. Aerosol optical and physical properties during
947 winter monsoon pollution transport in an urban environment. Environ. Sci. Pollut. Res. 21,
948 4977–4994.

949 Verma, S., Priyadharshini, B., Pani, S.K., Kumar, D.B., Faruqi, A.R., Bhanja, S.N., Mandal, M. 2016.
950 Aerosol extinction properties over coastal West Bengal Gangetic plain under inter-seasonal and
951 sea breeze influenced transport processes. Atmos. Res. 167, 224–236.

952 Wai, K.M., Lin, N.H., Wang, S.H., Dokiya, Y., 2008. Rainwater chemistry at a high-altitude station,
953 Mt. Lulin, Taiwan, Comparison with a background station, Mt. Fuji. J. Geophys. Res. 113,
954 D06305.

955 Wang, Q., Schwarz, J.P., Cao, J., Gao, R., Fahey, D.W., Hu, T., Huang, R.J., Han, Y., Shen, Z., 2014.
956 Black carbon aerosol characterization in a remote area of Qinghai–Tibetan Plateau, western
957 China. Sci. Total Environ. 479–480, 151–158.

958 Wang, Q.Y., Huang, R.J., Cao, J.J., Tie, X.X., Ni, H.Y., Zhou, Y.Q., Han, Y.M., Hu, T.F., Zhu, C.S.,
959 Feng, T., Li, N., Li, J.D., 2015. Black carbon aerosol in winter northeastern Qinghai-Tibetan
960 Plateau, China, the source, mixing state and optical property. Atmos. Chem. Phys. 15, 13059–
961 13069.

962 Wang, Z., Li, J., Wang, X., Pochanart, P., Akimoto, H., 2006. Modeling of regional high ozone
963 episode observed at two mountain sites (Mt. Tai and Huang) in East China. J. Atmos. Chem.
964 55(3), 253–272.

965 Weingartner, E., Saathoff, H., Schnaiter, M., Streit, N., Bitnar, B., Baltensperger, U., 2003.
966 Absorption of light by soot particles, determination of the absorption coefficient by means of
967 aethalometers. J. Aerosol Sci. 34, 1445–1463.

968 Xu, J.W., Martin, R.V., Morrow, A., Sharma, S., Huang, L., Leaitch, W.R., Burkart, J., Schulz, H.,
969 Zanatta, M., Willis, M.D., Henze, D.K., Lee, C.J., Herber, A.B., Abbatt, J.P.D., 2017. Source
970 attribution of Arctic black carbon constrained by aircraft and surface measurements. Atmos.
971 Chem. Phys. 17, 11971–11989.

972 Yamaji, K., Li, J., Uno, I., Kanaya, Y., Irie, H., Takigawa, M., Komazaki, Y., Pochanart, P., Liu, Y.,
973 Tanimoto, H., Ohara, T., Yan, X., Wang, Z., Akimoto, H., 2010. Impact of open crop residual
974 burning on air quality over Central Eastern China during the Mount Tai Experiment 2006
975 (MTX2006). Atmos. Chem. Phys. 10, 7353–7368.

976 Yashiro, H., Sugawara, S., Sudo, K., Aoki, S., Nakazawa, T., 2009. Temporal and spatial variations
977 of carbon monoxide over the western part of the Pacific Ocean. J. Geophys. Res. Atmos. 114,
978 D08305.

979 You, C., Gao, S., Xu, C., 2015. Biomass burning emissions contaminate winter snowfalls in urban
980 Beijing, A case study in 2012. Atmos. Pollut. Res. 6, 376–381.

981 Zellweger, C., Huglin, C., Klausen, J., Steinbacher, M., Vollmer, M., Buchmann, B., 2009. Inter-
982 comparison of four different carbon monoxide measurement techniques and evaluation of the
983 long-term carbon monoxide time series of Jungfraujoch. Atmos. Chem. Phys. 9, 3491–3503.

984 Zhai, P.M., Zhang, X.B., Wan, H., Pan, X.H., 2005. Trends in total precipitation and frequency of
985 daily precipitation extremes over China. J. Clim. 18, 1096–1108.

986 Zhang, Q., Streets, D.G., Carmichael, G.R., He, K.B., Huo, H., Kannari, A., Klimont, Z., Park, I. S.,
987 Reddy, S., Fu, J.S., Chen, D., Duan, L., Lei, Y., Wang, L.T., Yao, Z.L., 2009. Asian emissions in
988 2006 for the NASA INTEX-B mission, Atmos. Chem. Phys. 9, 5131–5153.

989 Zhang, X., Ming, J., Li, Zhongqin, Wang, F., Zhang, G., 2017. The online measured black carbon
990 aerosol and source orientations in the Nam Co region, Tibet. Environ. Sci. Pollut. Res. 24,
991 25021–25033.

992 Zhao, S., Ming, J., Xiao, C., Sun, W., Qin, X., 2012. A preliminary study on measurements of black
993 carbon in the atmosphere of northwest Qilian Shan. J. Environ. Sci. 24, 152–159.

994 Zhou, X., Gao, J., Wang, T., Wu, W., Wang, W., 2009. Measurement of black carbon aerosols near
995 two Chinese megacities and the implications for improving emission inventories. Atmos.
996 Environ. 43, 3918–3924.

997 **Table captions**

998 **Table 1**. Statistical data of seasonal meteorological parameters, EBC, and CO mass concentrations
999 measured at LABS during the study period.

1000 **Table 2.** Mean mass concentrations of EBC measured at various high-altitude locations in the world.
1001

1002 **Table 3**. Statistical results of ΔEBC-ΔCO scatterplots obtained during the study period.

1003

Figure captions

Fig. 1. (a) Geographical location of Taiwan and its adjacent Asian countries; (b) Terrain map of Taiwan and the red star shows the location of Mt Lulin; (c) Aerial view of Lulin Atmospheric Background Station (LABS). For interpretation of the references to color in this figure legend, the reader is referred to the web version of this article.

Fig. 2. Monthly mean (a) T (°C), (b) RH (%), (c) WS (m s^{-1}), and (d) rainfall (mm) at LABS during 2012–2014. Vertical bars indicate ± 1σ from the mean.

Fig. 3. Monthly distribution of air mass origins at LABS are shown by clusters of 5-day BTs arriving at ground level during 2012–2014. The numbers in each panel indicate the relative frequency (%) for each possible pathway in the month with such origins. Red dots represent the MODIS inferred fire counts.

Fig. 4. Monthly mean mass concentration of (a) EBC, and (b) CO at LABS during 2012–2014. Vertical bars indicate ± 1σ from the mean. Monthly background CO (refer to the section 3.4) values are also shown here.

Fig. 5. Scatterplot and linear regression results of the ΔEBC-ΔCO correlation for each month at LABS during the study period. The slope (mean ± standard error at 95% confidence interval) of the least-square regression line is the ΔEBC/ΔCO ratio in ng m^{-3} $ppbv^{-1}$ for the respective month.

Fig. 6. Scatterplot and linear regression results of the ΔEBC-ΔCO correlation for the episodic cases i.e., (a) Case#1, (b) Case#2, and (c) Case#3. The slope (mean ± standard error at 95% confidence interval) of the least-square regression line is the ΔEBC/ΔCO ratio in ng m^{-3} $ppbv^{-1}$ for the respective case.

Fig. 7. Representatives transport pathway of 5-day BT air mass arriving at ground level of LABS during (a) Case#1, (b) Case#2, and (c) Case#3. The solid star represents the LABS site. Vertical

information of aerosol subtypes along the CALIPSO satellite orbit (near to Taiwan region) for (d) Case#1, (e) Case#2, and (f) Case#3. Black color blocks indicate the presence of "elevated smoke aerosols". For interpretation of the references to color in this figure legend, the reader is referred to the web version of this article.

Fig. 8. Comparison of ΔEBC/ΔCO ratios obtained at Mt. Lulin with other worldwide locations.

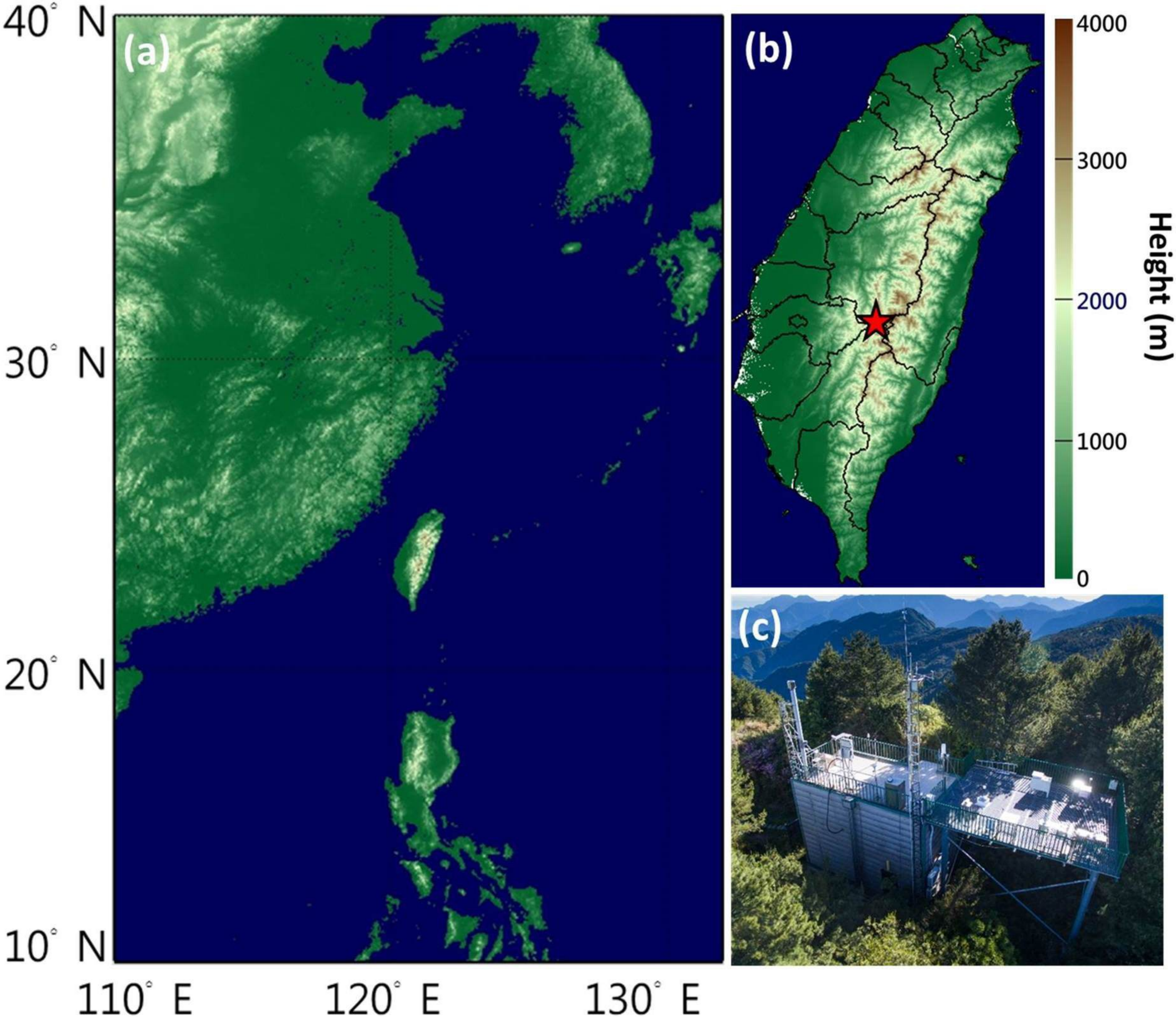
40° N
30° N
20° N
10° N
110° E
120° E
130° E
(a)
(b)
(c)
4000
3000
2000
1000
0
Height (m)

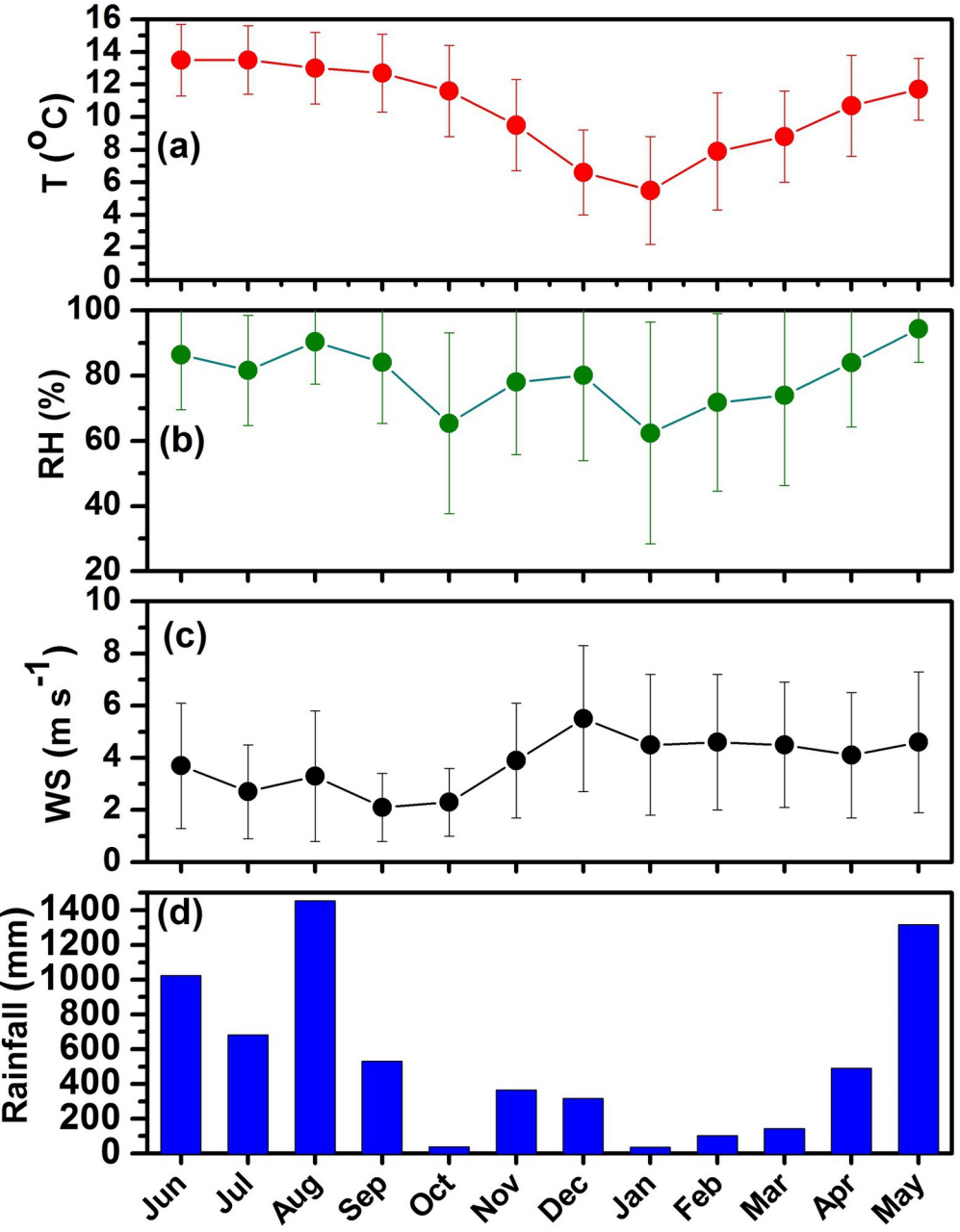
T (°C)
(a)
RH (%)
(b)
WS (m s-1)
(c)
Rainfall (mm)
(d)
Jun
Jul
Aug
Sep
Oct
Nov
Dec
Jan
Feb
Mar
Apr
May

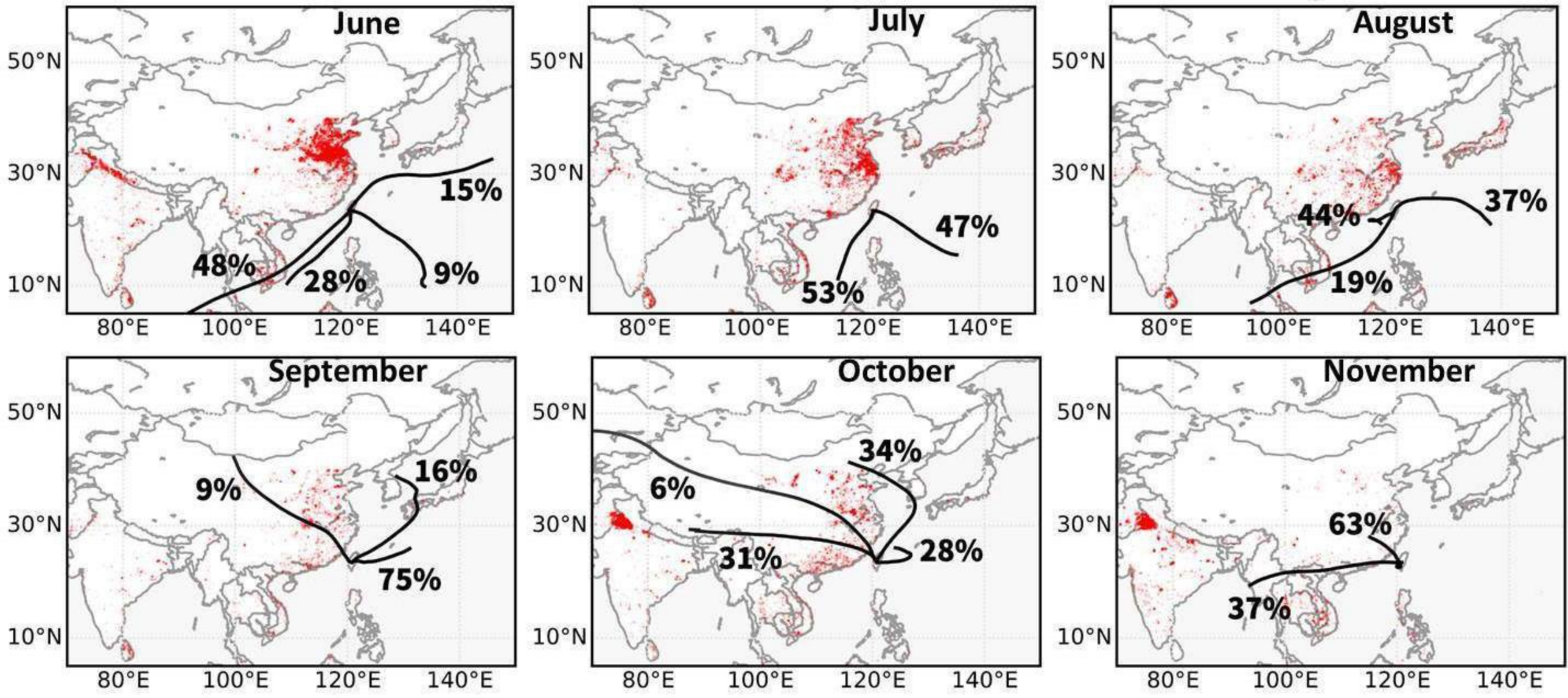
June
15%
48%
28%
9%
July
47%
53%
August
44%
37%
19%
September
9%
16%
75%
October
34%
6%
31%
28%
November
63%
37%
December
3%
39%
32%
26%
January
38%
27%
35%
February
23%
37%
40%
March
15%
44%
41%
April
18%
14%
68%
May
32%
19%
22%
27%
50°N
30°N
10°N
80°E
100°E
120°E
140°E

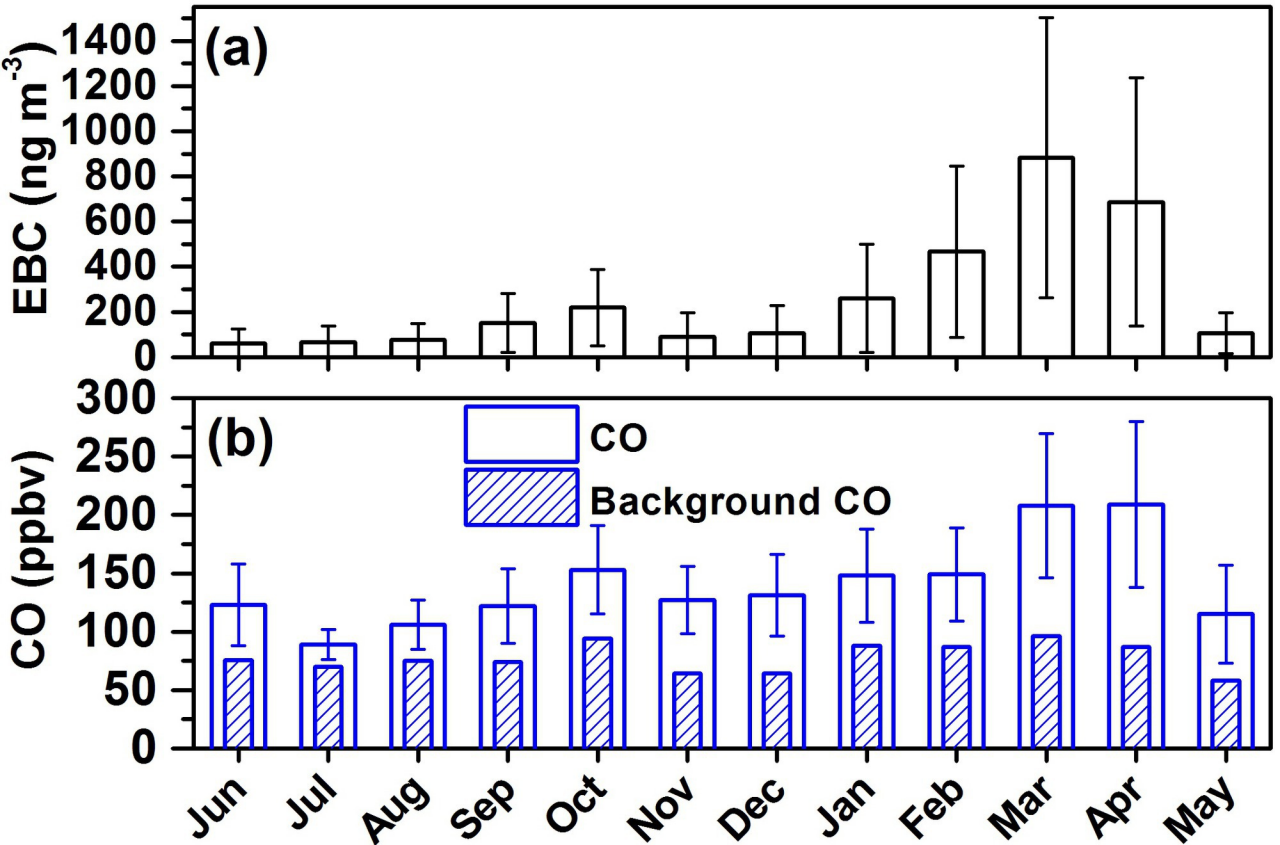
(a)
EBC (ng m-3)
1400
1200
1000
800
600
400
200
0
(b)
CO (ppbv)
CO
Background CO
300
250
200
150
100
50
0
Jun
Jul
Aug
Sep
Oct
Nov
Dec
Jan
Feb
Mar
Apr
May

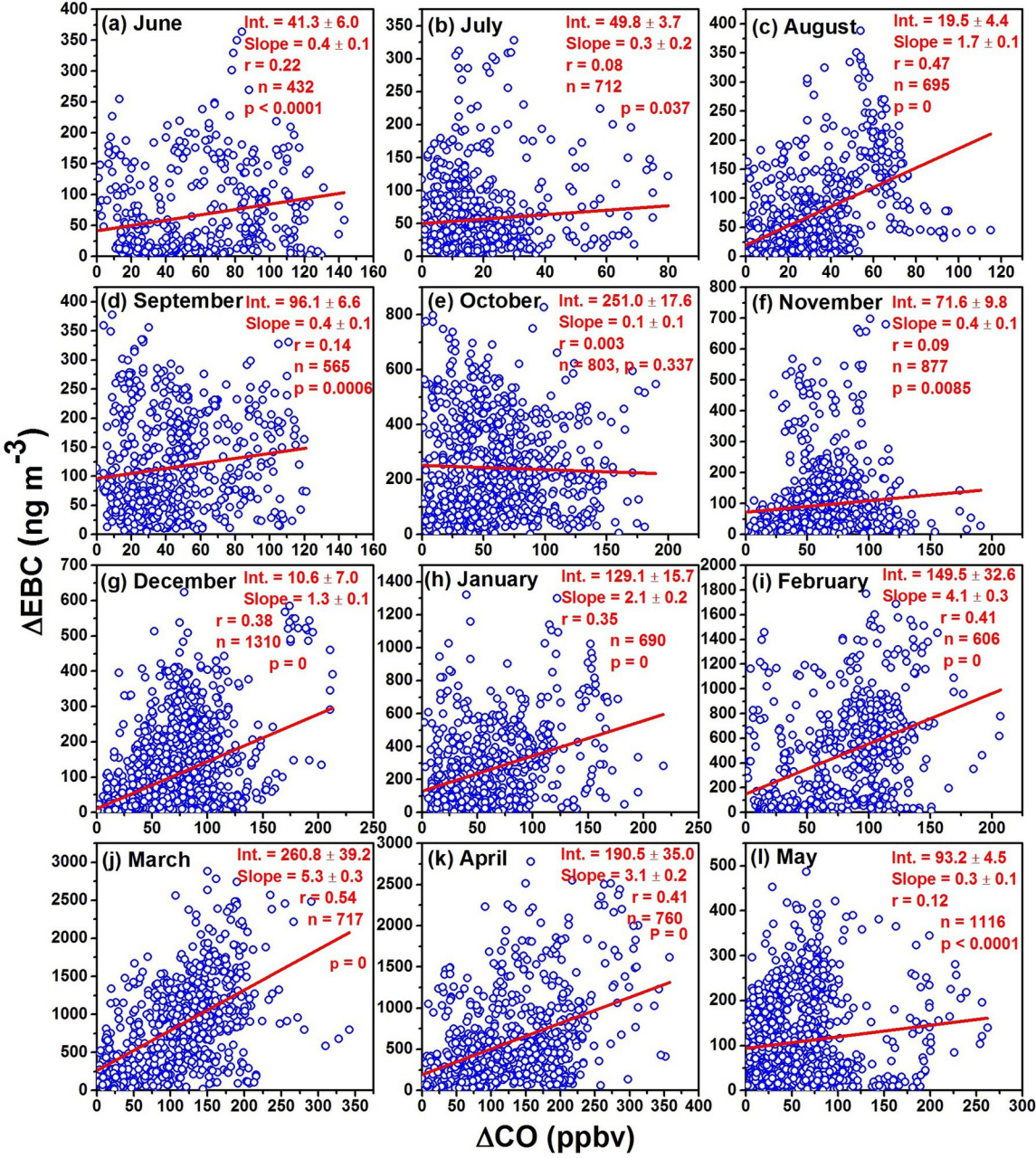
(a) June
Int. = 41.3 ± 6.0
Slope = 0.4 ± 0.1
r = 0.22
n = 432
p < 0.0001
(b) July
Int. = 49.8 ± 3.7
Slope = 0.3 ± 0.2
r = 0.08
n = 712
p = 0.037
(c) August
Int. = 19.5 ± 4.4
Slope = 1.7 ± 0.1
r = 0.47
n = 695
p = 0
(d) September
Int. = 96.1 ± 6.6
Slope = 0.4 ± 0.1
r = 0.14
n = 565
p = 0.0006
(e) October
Int. = 251.0 ± 17.6
Slope = 0.1 ± 0.1
r = 0.003
n = 803, p = 0.337
(f) November
Int. = 71.6 ± 9.8
Slope = 0.4 ± 0.1
r = 0.09
n = 877
p = 0.0085
(g) December
Int. = 10.6 ± 7.0
Slope = 1.3 ± 0.1
r = 0.38
n = 1310
p = 0
(h) January
Int. = 129.1 ± 15.7
Slope = 2.1 ± 0.2
r = 0.35
n = 690
p = 0
(i) February
Int. = 149.5 ± 32.6
Slope = 4.1 ± 0.3
r = 0.41
n = 606
p = 0
(j) March
Int. = 260.8 ± 39.2
Slope = 5.3 ± 0.3
r = 0.54
n = 717
p = 0
(k) April
Int. = 190.5 ± 35.0
Slope = 3.1 ± 0.2
r = 0.41
n = 760
P = 0
(l) May
Int. = 93.2 ± 4.5
Slope = 0.3 ± 0.1
r = 0.12
n = 1116
p < 0.0001
ΔEBC (ng m-3)
ΔCO (ppbv)

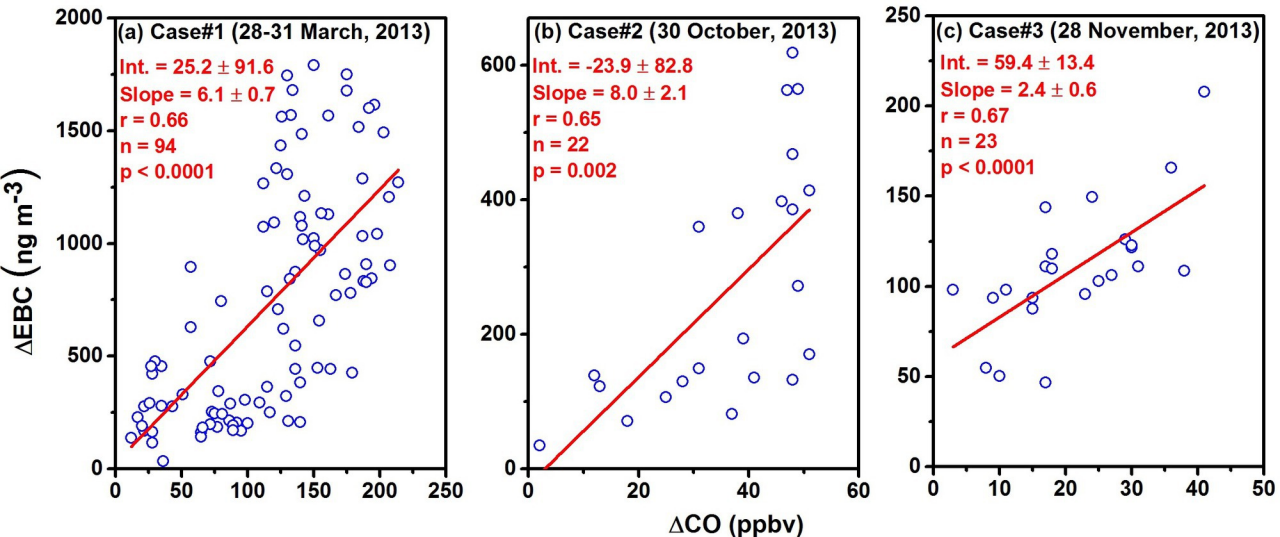
(a) Case#1 (28-31 March, 2013)
Int. = 25.2 ± 91.6
Slope = 6.1 ± 0.7
r = 0.66
n = 94
p < 0.0001
(b) Case#2 (30 October, 2013)
Int. = -23.9 ± 82.8
Slope = 8.0 ± 2.1
r = 0.65
n = 22
p = 0.002
(c) Case#3 (28 November, 2013)
Int. = 59.4 ± 13.4
Slope = 2.4 ± 0.6
r = 0.67
n = 23
p < 0.0001
ΔEBC (ng m-3)
ΔCO (ppbv)

(a)

Source ★ at 23.47 N 120.87 E

hPa

723

Job ID: 196073 Job Start: Thu Jun 21 09:48:07 UTC 2018
Source 1 lat.: 23.470000 lon.: 120.870000 height: 2862 m AMSL

Trajectory Direction: Backward Duration: 120 hrs
Vertical Motion Calculation Method: Model Vertical Velocity
Meteorology: 0000Z 22 Mar 2013 - GDAS1

(b)

Source ★ at 23.47 N 120.87 E

hPa

721

Job ID: 11408 Job Start: Tue Jul 3 08:03:06 UTC 2018
Source 1 lat.: 23.470000 lon.: 120.870000 height: 2862 m AMSL

Trajectory Direction: Backward Duration: 120 hrs
Vertical Motion Calculation Method: Model Vertical Velocity
Meteorology: 0000Z 30 Oct 2013 - GDAS0p5

(c)

Source ★ at 23.47 N 120.87 E

hPa

714

Job ID: 1360 Job Start: Tue Jul 3 07:44:02 UTC 2018
Source 1 lat.: 23.470000 lon.: 120.870000 height: 2862 m AMSL

Trajectory Direction: Backward Duration: 120 hrs
Vertical Motion Calculation Method: Model Vertical Velocity
Meteorology: 0000Z 28 Nov 2013 - GDAS0p5

(d)

Aerosol Subtype UTC: 2013-03-28 06:04:39.9 to 2013-03-28 06:18:08.6 Version: 4.10 Standard Daytime

UTC: 2013-03-28 05-37-43 Version: 4.10 Standard Daytime

Altitude, km

Lat 9.78 15.89 22.00 28.09 34.17 40.23 46.26 52.26 58.16
Lon 113.63 112.28 110.88 109.38 107.76 105.95 103.88 101.39 98.29

N/A = not applicable 1 = marine 2 = dust 3 = polluted continental/smoke 4 = clean continental 5 = polluted dust 6 = elevated smoke 7 = dusty marine
8 = PSC aerosol 9 = volcanic ash 10 = sulfate/other

(e)

Aerosol Subtype UTC: 2013-10-30 17:20:44.2 to 2013-10-30 17:34:12.9 Version: 4.10 Standard Nighttime

UTC: 2013-10-30 17-07-16 Version: 4.10 Standard Nighttime

Altitude, km

Lat 45.84 39.81 33.75 27.67 21.57 15.47 9.36 3.24 -2.83
Lon 134.43 132.38 130.59 128.99 127.50 126.10 124.76 123.45 122.16

N/A = not applicable 1 = marine 2 = dust 3 = polluted continental/smoke 4 = clean continental 5 = polluted dust 6 = elevated smoke 7 = dusty marine
8 = PSC aerosol 9 = volcanic ash 10 = sulfate/other

(f)

Aerosol Subtype UTC: 2013-11-28 18:26:15.3 to 2013-11-28 18:39:44.0 Version: 4.10 Standard Nighttime

UTC: 2013-11-28 18-12-49 Version: 4.10 Standard Nighttime

Altitude, km

Lat 54.29 48.31 42.29 36.24 30.17 24.08 17.99 11.88 5.81
Lon 121.10 118.43 116.24 114.35 112.68 111.15 109.72 108.35 107.04

N/A = not applicable 1 = marine 2 = dust 3 = polluted continental/smoke 4 = clean continental 5 = polluted dust 6 = elevated smoke 7 = dusty marine
8 = PSC aerosol 9 = volcanic ash 10 = sulfate/other

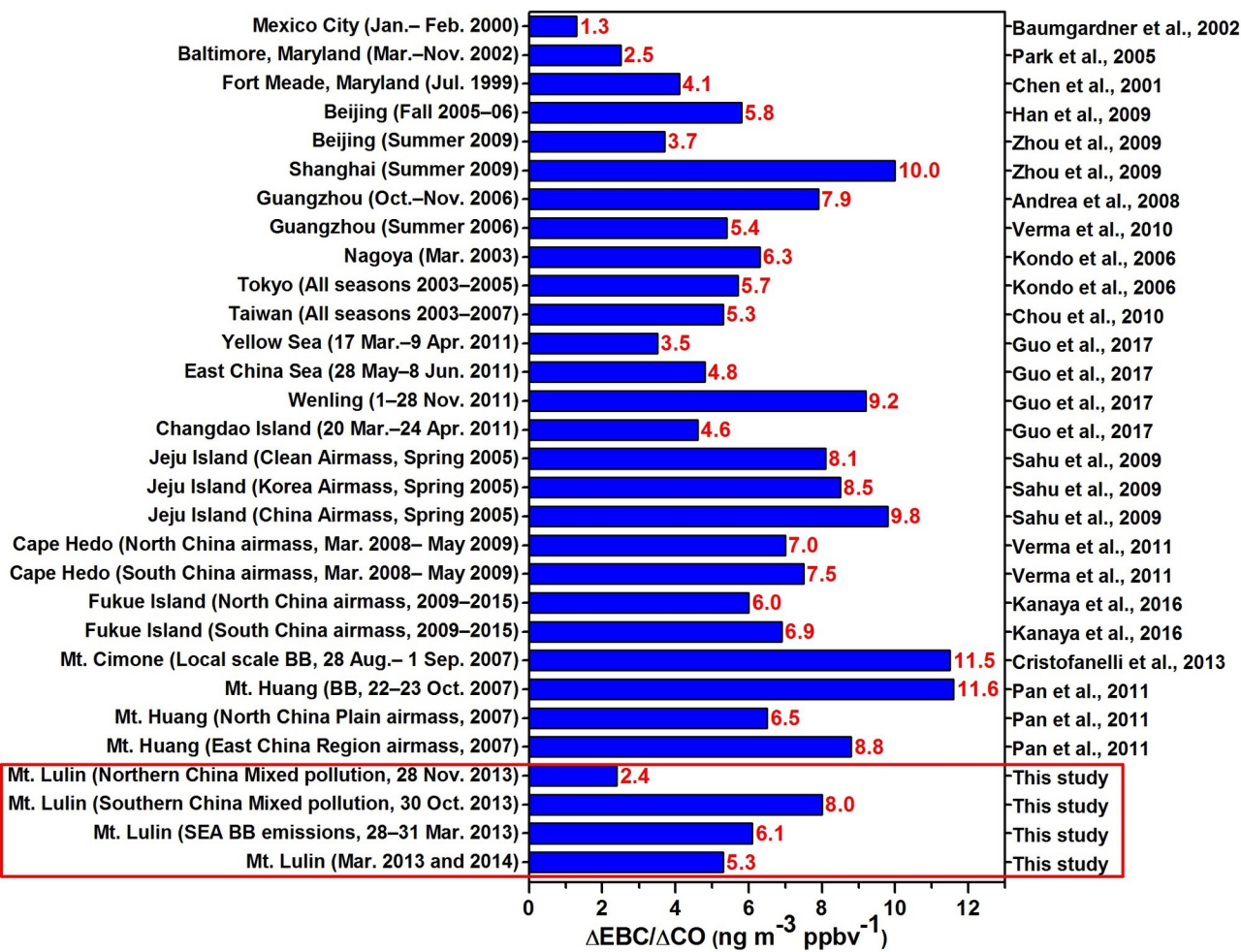
Mexico City (Jan.– Feb. 2000) 1.3 Baumgardner et al., 2002
Baltimore, Maryland (Mar.–Nov. 2002) 2.5 Park et al., 2005
Fort Meade, Maryland (Jul. 1999) 4.1 Chen et al., 2001
Beijing (Fall 2005–06) 5.8 Han et al., 2009
Beijing (Summer 2009) 3.7 Zhou et al., 2009
Shanghai (Summer 2009) 10.0 Zhou et al., 2009
Guangzhou (Oct.–Nov. 2006) 7.9 Andrea et al., 2008
Guangzhou (Summer 2006) 5.4 Verma et al., 2010
Nagoya (Mar. 2003) 6.3 Kondo et al., 2006
Tokyo (All seasons 2003–2005) 5.7 Kondo et al., 2006
Taiwan (All seasons 2003–2007) 5.3 Chou et al., 2010
Yellow Sea (17 Mar.–9 Apr. 2011) 3.5 Guo et al., 2017
East China Sea (28 May–8 Jun. 2011) 4.8 Guo et al., 2017
Wenling (1–28 Nov. 2011) 9.2 Guo et al., 2017
Changdao Island (20 Mar.–24 Apr. 2011) 4.6 Guo et al., 2017
Jeju Island (Clean Airmass, Spring 2005) 8.1 Sahu et al., 2009
Jeju Island (Korea Airmass, Spring 2005) 8.5 Sahu et al., 2009
Jeju Island (China Airmass, Spring 2005) 9.8 Sahu et al., 2009
Cape Hedo (North China airmass, Mar. 2008– May 2009) 7.0 Verma et al., 2011
Cape Hedo (South China airmass, Mar. 2008– May 2009) 7.5 Verma et al., 2011
Fukue Island (North China airmass, 2009–2015) 6.0 Kanaya et al., 2016
Fukue Island (South China airmass, 2009–2015) 6.9 Kanaya et al., 2016
Mt. Cimone (Local scale BB, 28 Aug.– 1 Sep. 2007) 11.5 Cristofanelli et al., 2013
Mt. Huang (BB, 22–23 Oct. 2007) 11.6 Pan et al., 2011
Mt. Huang (North China Plain airmass, 2007) 6.5 Pan et al., 2011
Mt. Huang (East China Region airmass, 2007) 8.8 Pan et al., 2011
Mt. Lulin (Northern China Mixed pollution, 28 Nov. 2013) 2.4 This study
Mt. Lulin (Southern China Mixed pollution, 30 Oct. 2013) 8.0 This study
Mt. Lulin (SEA BB emissions, 28–31 Mar. 2013) 6.1 This study
Mt. Lulin (Mar. 2013 and 2014) 5.3 This study
0 2 4 6 8 10 12
ΔEBC/ΔCO (ng m-3 ppbv-1)

Table 1: Statistical data of seasonal meteorological parameters, EBC, and CO mass concentrations measured at LABS during the study period.

Parameters	Summer			Autumn			Winter			Spring		
	Mean ± 1σ	Median	IQR[#]	Mean ± 1σ	Median	IQR	Mean ± 1σ	Median	IQR[#]	Mean ± 1σ	Median	IQR[#]
T (°C)	13 ± 2	13	12–15	11 ± 3	11	9–13	7 ± 3	7	4–9	10 ± 3	10	8–12
RH (%)	86 ± 16	92	78–100	76 ± 24	83	62–97	71 ± 30	81	53–100	84 ± 22	95	75–100
WS (m s^{-1})	3.2 ± 2.3	2.5	1.5–4.3	2.8 ± 1.9	2.3	1.4–3.6	4.9 ± 2.7	4.5	2.7–6.8	4.4 ± 2.5	4.0	2.4–6.2
P (hPa)	723 ± 3	724	722–726	725 ± 2	725	724–727	724 ± 2	724	723–726	725 ± 2	725	724–726
EBC (ng m^{-3})	68 ± 71	39	16–102	152 ± 148	104	38–216	252 ± 295	140	34–370	563 ± 585	348	106–863
CO (ppbv)	104 ± 27	95	85–115	135 ± 36	130	109–156	142 ± 39	137	112–167	167 ± 74	150	105–222

[#] IQR: Interquartile range = 25–75 percentile.

Table 2: Mean mass concentrations of EBC measured at various high-altitude locations in the world.

Locations	Altitude (m)	Period	Elevated BC sources	Method	EBC (ng m^{-3})	References
Sinhagad, Western Ghats in India	1450	Apr. – May, 2009	Prevailing meteorology and certain local burning activities	AE	860	Raju et al., 2011
DAK, Northern Thailand	1536	Mar. 2013	Agricultural residue burning	AE	5430	Hsiao et al., 2016
Godavari, Central Nepal	1600	Oct. 2005 – Dec. 2007	Mainly influenced by local combustion sources	PSAP	560	Engstrom and Leck, 2017
Tengchong County, Southeast Tibet	1640	Apr.–May 2004	Influenced by Southeast Asia and local domestic activities	AE	420	Engling et al., 2011
Mt. Huang, Eastern China	1840	Jun. 2006 – May 2009	Large-scale burning of crop residues	MAAP	1004	Pan et al., 2011
Manora Peak, Central Himalayas	1958	Nov. 2004 – Dec. 2007	Convective boundary layer and increased local emissions	AE	990	Dumka et al., 2010
Darjeeling, Eastern Himalaya	2200	Jan. 2010 – Dec. 2011	Local anthropogenic activities and long-range transport from Pakistan, Afghanistan and Indo-Gangetic Plain	AE	3450	Sarkar et al., 2015
Ooty, Western Ghats of Southern India	2520	Apr. 2010 – May 2012	Influenced by anthropogenically polluted metropolitan cities like Chennai and Bangalore in India	AE	610	Udayasoorian et al., 2014
LABS, Mt. Lulin, Central Taiwan	**2862**	**Jun. 2012 – May 2014**	**Asian continental outflow and long-range transport of emissions from South and Southeast Asia**	**AE**	**275**	**This study**
		Mar. 2013 and 2014	**Attributed to westerly winds coupled with BB emissions from Southeast Asia**		**883**	
Linzhi, Southeast Tibet	3300	Jan. 2009	Primarily from Eastern India and Bangladesh	AE	760	Cao et al., 2010
Mt.Waliguan, Northeastern Tibetan Plateau	4000	Oct.–Nov. 1997/Jan. 1998	Influenced by northeastern cities of China	AE	270	Ma et al., 2003
Qilian Shan, Northwest China	4214	May 2009 – Mar. 2011	Influenced by northwest wind	AE	50	Zhao et al., 2012
Hanle, Western Himalayas	4520	Aug. 2009 – Jul. 2010	Influenced by the advection from West and Southwest Asia	AE	80	Babu et al., 2011
Nam Co, Central Tibet	4730	Oct. 2010 – Oct. 2014	Local anthropogenic activities, such as indigenous Tibetan burning animal waste and tourism traffic	AE	74	Zhang et al., 2017
NCO-P, Southern Himalayas	5079	Mar. 2006 – Mar. 2008	Regional circulation and westerly air masses from the Middle East	MAAP	160	Marinoni et al., 2010

Note: The content of this study are shown as bold. AE: Aethalometer; PSAP: Particle Soot Absorption Photometer; MAAP: Multi-Angle Absorption Photometer.

Table 3: Statistical results of ΔEBC-ΔCO scatterplots during the study period.

Months/Cases	n [a]	r [b]	p [c]	Slope (ΔEBC/ΔCO ratio)	
				[d] ng m^{-3} $ppbv^{-1}$	[e] g g^{-1}
August	695	0.47	< 0.0001	1.7 ± 0.1	2.4×10^{-3}
December	1310	0.38	0	1.3 ± 0.1	1.8×10^{-3}
January	690	0.35	0	2.1 ± 0.2	2.9×10^{-3}
February	606	0.41	0	4.1 ± 0.3	5.6×10^{-3}
March	717	0.54	0	5.3 ± 0.3	7.3×10^{-3}
April	760	0.41	0	3.1 ± 0.2	4.3×10^{-3}
Case#1	94	0.66	< 0.0001	6.1 ± 0.7	8.4×10^{-3}
Case#2	22	0.65	0.002	8.0 ± 2.1	11.1×10^{-3}
Case#3	23	0.67	< 0.0001	2.4 ± 0.6	3.3×10^{-3}

[a]: number of pairs of hourly averaged data; [b]: at the 95% significance level; [c]: significance level of the slope; [d]: values are written as mean ± standard error at 95% confidence interval; [e]: values of ΔEBC/ΔCO ratios are written as grams of carbon as EBC per gram of carbon as CO